Negative electron affinity and the diamond surface

Robert van den Bogaerde
09/07/2012

Contents

1.0 – Introduction

1.1 – Diamond
1.1.1 – Diamond surfaces
1.1.2 – Chemical vapour deposition

1.2 – Negative electron affinity
1.2.1 – NEA in other materials
1.2.2 – NEA in diamond

1.3 – Applications
1.3.1 – Thermionic emission
1.3.2 – Field emission
1.3.3 – Secondary emission

2.0 – Experimental

2.1 – Sample preparation
2.1.1 – Acid cleaning
2.1.2 – UVO cleaning
2.1.3 – Metal coating
2.1.4 – Acid washing

2.2 – Sample analysis
2.2.1 – Scanning electron microscopy (SEM)
2.2.2 – Energy-dispersive X-ray spectroscopy (EDX)
2.2.3 – Atomic force microscopy (AFM)
2.2.4 – Raman spectroscopy
2.2.5 – Conductivity measurements

3.0 – Results and discussion

3.1 – Surface morphology and composition
3.1.1 – Magnesium coating
3.1.2 – Titanium coating
3.1.3 – Chromium coating
3.1.4 – Aluminium coating
3.1.5 – Nickel coating

3.2 – Raman results
3.3 – AFM results

3.4 – Conductivity results

4.0 – Conclusions

5.0 – Future work

6.0 – Acknowledgements

7.0 – Appendix

7.1 – SEM data
7.2 – EDX data
7.3 – Raman spectra
7.4 – AFM data

8.0 - References

1.0 – Introduction

1.1 – Diamond

Diamond is a unique material with many interesting properties that has fascinated man for centuries. Until the 17th century, there were several proposals on the origin of diamond, including the notion that they were pieces of ice that had been frozen for a very long time. [1] It is now known that diamond is in fact an allotrope of carbon, more of which are shown in figure 1.

Diamond is the hardest material found in nature, defined as 10 on the Mohs scale of hardness, which is the maximum value. [2] It has a high refractive index (2.417 at 589 nm) and a high dispersion [3], as well as being completely transparent in the wavelength range 225 nm to 2.5 μm, which makes diamond desirable as a gemstone. [4] Diamond has the highest thermal conductivity of any bulk material, over six times that of copper at room temperature. [4]

Diamond is also a very stable material. It can withstand temperatures of up to 850°C in air, but oxidises to CO_2 if heated above that. [5] Under an atmosphere of Ar, it can be heated to 1700°C and remain intact. [6] Diamond is stable to most chemical reagents, including all acids. [2] However, it can be etched by alkalis and some strong oxidants at temperatures exceeding 380°C. [7]

In addition, diamond has some remarkable electrical properties. Diamond has a wide band gap of 5.47 eV [8], and boron doping introduces bands within this which creates many possible uses for diamond as a semiconductor, given its stability, thermal conductivity and hardness. Highly boron-doped diamond can also act as a superconductor; the highest reported transition temperature is 11.4 K. [9]

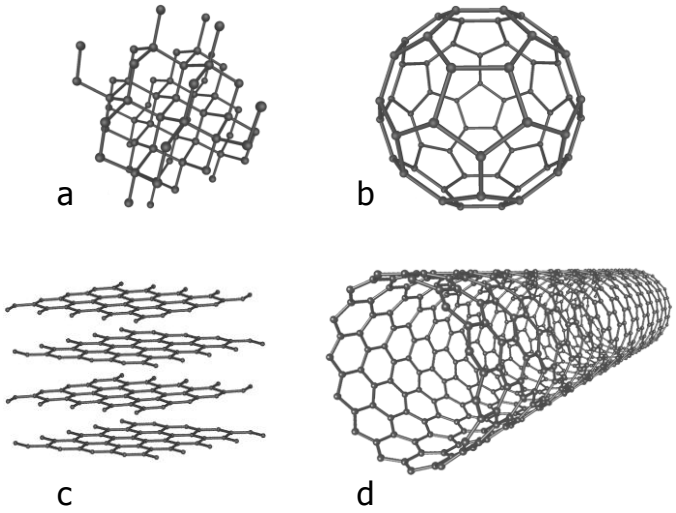

Figure 1. Allotropes of carbon, a: diamond, b: Buckminster fullerene, c: graphite, d: carbon nanotube

1.1.1 – Diamond surfaces

Three main surfaces of diamond exist: (100), (110) and (111). The (100) surface is unique in having two dangling bonds per surface atom, while the (110) and (111) surfaces only have one. As it is possible to grow an almost atomically smooth (100) surface, the (100) surface is the focus of research on diamond surfaces. [10] A polished diamond surface is terminated with H atoms which produces a 1x1 low-energy electron diffraction (LEED) pattern for (110) and (111) surfaces, indicating a fully hydrogenated surface. [4] The (100) surface may exist as a monohydrogenated or dihydrogenated surface, with 1x2 and 1x1 LEED diffraction patterns respectively. However, due to steric hindrance the dihydrogenated (100) surface is unstable because the surface is so dense, and only the monohydrogenated surface is seen in practice. [11] This has also been confirmed by high-resolution electron energy loss spectroscopy (HREELS). [12] Figure 2 shows the structure of C(100)-(2x1):H and C(100)-(1x1):2H surfaces.

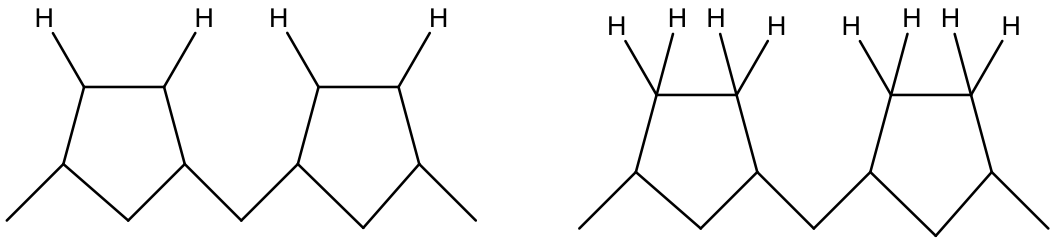

Figure 2. Structure of C(100)-(2x1):H and C(100)-(1x1):2H surfaces. Due to their high density at the surface, steric clashes between H atoms on the (1x1):2H surface make this structure very unstable.

At temperatures over 900°C, the C-H bonds are broken and the H termination is lost. The surface reconstructs, with concurrent formation of occupied and unoccupied band gap states. [4]

1.1.2 – Chemical vapour deposition

Chemical vapour deposition is one of several methods for synthesising diamond, notable because it is carried out at far lower temperatures and pressures than older high-pressure high-temperature synthesis methods. CVD diamonds synthesis involves feeding source gases into a reactor, energising them and providing a suitable substrate for diamond to grow on. The source gases include a hydrocarbon source, usually methane, and hydrogen in large excess. [13] One of the advantages of CVD over other techniques is that the composition of the diamond produced can be precisely controlled by modifying the source gases. Dopants can be introduced, for example boron to create p-type semiconducting diamond. In addition, thin films of diamond can be synthesised over large areas, leading to many potentially useful applications.

1.2 – Negative electron affinity

A surface with negative electron affinity is defined as the conduction band minimum, E_c being above the vacuum level, E_0. Figure 3 shows the band diagram for an NEA surface. The band gap, E_g is the difference between E_c and the valence band maximum, E_v. The electron affinity, χ, is the difference between E_0, and E_c at the surface of the material. The work function, ϕ, is the difference between the Fermi level, E_f, and E_0. Therefore, if $\chi < E_g$, the surface displays NEA. Therefore, an electron with energy greater than or equal to E_c can be emitted into the vacuum no barrier at the surface. [14, 15] The band bending seen near the surface is due to the presence of surface states. [16]

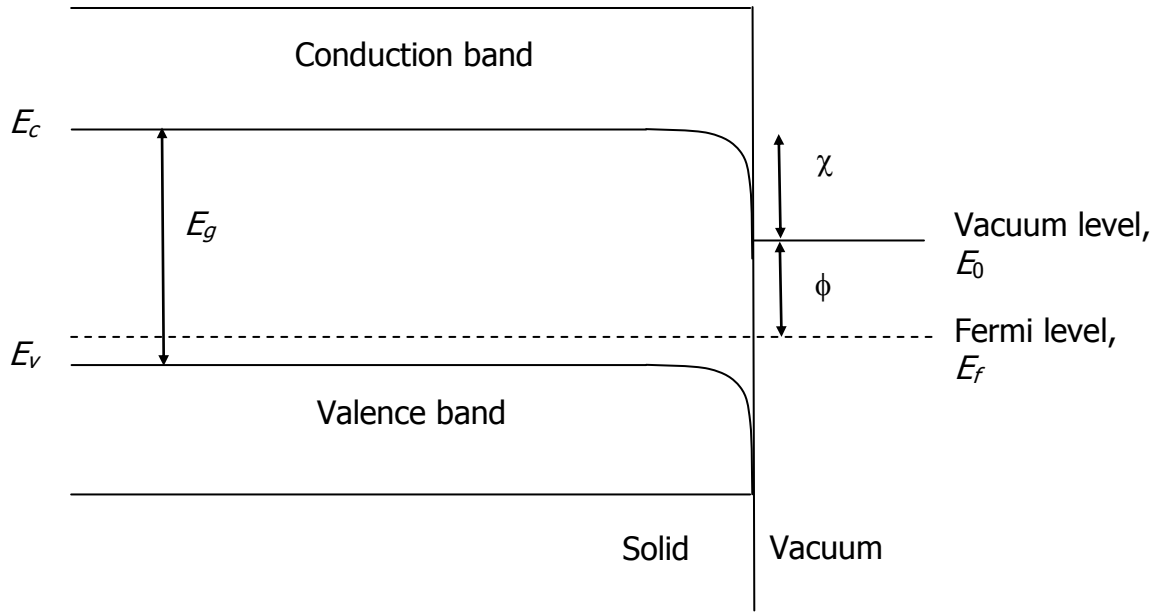

Figure 3. Band diagram showing negative electron affinity conditions at a p-type surface in relation to band gap E_g, electron affinity χ and work function ϕ

The two key requirements of an NEA material are that it has a high level of crystalline perfection, carefully controlled composition and impurity presence. This is necessary for the correct bulk properties to be present. The other requirement is that the surface of the material is prepared to give a low work function, ϕ. [17] Diamond lends itself well to these requirements as CVD techniques can precisely control the composition of the crystal or film produced.

1.2.1 – NEA in other materials

NEA was first discovered in a non-diamond material. To achieve NEA in materials other than diamond, the work function of a semiconductor is reduced by adsorption of an electropositive element to the atomically clean surface. The most commonly used semiconductors are III-V type, and the

most commonly used adsorbate is Cs. [15] Development began in the 1960s with the first recorded NEA material discovered by the U.S. Army in 1963. [18] Different materials and adsorbates were discovered throughout the late 1960s and 1970s, such as GaAs, GaP, InP and many more. Adsorbates include Cs, Cs-O, Cs-F and Rb-O.

A non III-V material that can exhibit NEA is Si, first demonstrated in 1970 by Martinelli. [19] This has several advantages, such as silicon's abundance in the Earth's crust and the fact it is a pure element, simplifying manufacturing processes and avoiding thermal unmixing. Impurity density is very low so a very fine circuit can be built compared with GaAs and other III-V materials. However, GaAs has a wider band gap that makes it less heat sensitive. This also makes it insensitive to radiation, which lends it to uses in space electronics and high-powered applications.

1.2.2 – NEA in diamond

NEA in diamond was first demonstrated in 1979 by Himpsel et al, with work done on the (111) surface. [20] In 1994, Van der Weide et al demonstrated NEA at the (100) surface. [21] Diamond's properties make it a superior material compared with III-V semiconductors or silicon, as these tend to be far less stable than diamond at high temperatures, and are chemically sensitive.

NEA in diamond comes about due to a dipole present at the surface. This dipole arises from a species other than carbon terminating the surface. This has been confirmed by Cui et al with practical research [22] as well as a theoretical study by Rutter et al. [14] As mentioned earlier, diamond is normally terminated with H. H has a Pauling electronegativity of 2.20 and C has a value of 2.55. Therefore, there is a small dipole present at the surface. This dipole provides a potential step that pulls E_0 below E_c over a distance that corresponds to the CH bond length. [23]

Diamond surfaces can be terminated with many other species. For example, when terminated with O, there is a larger dipole present as O has a Pauling electronegativity of 3.44. However, as this dipole is in the other direction to H-terminated diamond, PEA is observed at the surface. [24] If the surface is terminated with OH molecules, there is a larger NEA than with simple H termination, because the OH bond produces a dipole that opposes the CO bond and enhances the NEA. [14] Table 1 presents experimentally determined NEA values for various diamond surfaces and terminations.

Surface	χ (eV)	Source
C(100)-(2x1)	0.75 1.3 0.5	Baumann et al [25] Diederich et al [26] Maier et al [23]
C(100)-(2x1):H	–0.8 ≤ –1.0 –1.3	Bandis and Pate [27] Diederich et al [26] Maier et al [23]
C(100)-(1x1):O	1.0 – 1.5 0.64 1.7	Baumann et al [25] Wang et al [28] Maier et al [23]
C(100)-(2x1):OH	≤ –1.1	Diederich et al [29]
C(100)-(2x1):CsO	–0.85	Pickett [30]
C(100)-(1x1):SiO_2	2.3	Geis et al [31]
C(110)-(1x1):H	≤ –1.0	Diederich et al [29]
C(111)-(2x1)	0.5 0.5 0.38	Bandis and Pate [32] Baumann et al [25] Cui et al [22]
C(111)-(1x1):H	≤ –0.7 ≤ –0.9 –1.27	Bandis and Pate [32] Diederich et al [26] Cui et al [22]
C(111)-(1x1):SiO_2	–0.7	Geis et al [31]

Table 1. Experimental NEA values for different diamond surfaces and terminations.

There is significant variation amongst some of the data shown in table 1. This could be due to differing experimental methods or problems with the quality of the diamond crystal used.

1.3 – Applications

Diamond's properties coupled with NEA make possible a number of promising real-world applications of this technology.

1.3.1 – Thermionic emission

Thermionic emission refers to the heat-induced flow of electrons from a surface. The electrons must overcome an energy barrier, which is the work function of the material, ϕ. The main use of this effect is electricity generation from heat, known as thermionic conversion. The first thermionic converter was demonstrated by Hernqvist et al in 1958. [33] There was much interest from the Russians in using the technology in nuclear reactors in space for power generation, [34] but this died down after the space program was cut back after the Cold War.

Current thermionic emitters rely on temperatures over 1000°C which limits their uses significantly. The Richardson equation (equation 1) indicates that a

material with a low work function ϕ has a high electron emission current density J. Due to its NEA, diamond also has a very low work function, making it a suitable material. This can be modified by doping the crystal through CVD techniques and changing the adsorbate as detailed earlier.

$$J = A_G T^2 e^{\frac{-\varphi}{k_B T}} \quad (1)$$

Diamond with CsO adsorbed onto the surface has an extremely low work function of 1.25 eV, owing to the large Cs-O dipole. [30, 35] The layer is stable in air [36], but decomposes around 400°C, unfortunately making it unsuitable for thermionic applications. [35]

N-doped nanocrystalline diamond has been studied and found to have a reasonably high Richardson's constant A_G of 70, and a very low work function of 1.99 eV. [37] A study of a single-crystal N-doped diamond found a work function of 2.4 eV. [38] The N impurities in the diamond act as electron donors, [22] and this combined with NEA at the surface makes this a material with great potential as a thermionic convertor. P-doped nanocrystalline diamond has been studied, and was found to have a work function of 0.9 eV, possibly the lowest ever reported for any material. All these studies have in common the significantly lower operating temperature of the device than current technology, which is one of the main problems with it. Further research is currently being done into other adsorbates that have a low work function and sufficient high temperature stability, for example Li on the (100) diamond surface by O'Donnell et al. [39]

If a heat-stable diamond surface with low enough work function can be manufactured, this would lend itself very well to concentrated solar power systems. The sun's energy could be focused onto a diamond thermionic device by mirrors and lenses to provide a high enough heat level to generate electricity. It is hoped that this will be significantly more efficient than existing Si based solar cells which have a theoretical maximal efficiency of 33.7%, [40] with the best commercial products converting around 25% of the sunlight to electricity. This could significantly reduce human dependence on fossil fuels.

1.3.2 – Field emission

Field emission refers to the emission of electrons induced by an electrostatic field, most commonly from a surface to vacuum. This is used in a variety of applications, such as electron microscopy, cathode ray tubes, cold cathode fluorescent lighting and field emission displays. Diamond's chemical inertness in particular makes it an ideal material for field emission devices. The more electropositive the adsorbate, the better the emission properties, both in terms of low threshold voltage and high emission currents. This is due to surface dipoles as discussed earlier. Geis et al [41] fabricated efficient diamond field emission cathodes with diamond grit, along with Ni and Cs salts to

improve emission. Electrons were injected into vacuum with little to no applied electric field, 0-1 V μm^{-1}. They reached the current densities required for flat panel displays at gate voltages of 10-15 V.

Sakai et al [42] developed a functional cold discharge cathode lamp from B-doped CVD diamond that uses 13% less power than conventional Mo cold cathode fluorescent lamps. A problem with normal CCFLs is cathode fall, V_C. This is a large voltage drop in front of the cathode during discharge, which means they must be operate at higher voltages to function correctly. This can be seen in figure 4. Diamond's high secondary electron emission yield due to NEA and the p-type semiconductivity of B-doped material make it an ideal candidate to replace traditional cold cathodes. The device developed by Sakai et al showed a 35% smaller cathode fall than that seen with Mo. CCFLs are used mostly for backlighting in LCD screens and TVs, so any efficiency improvement would be highly desirable.

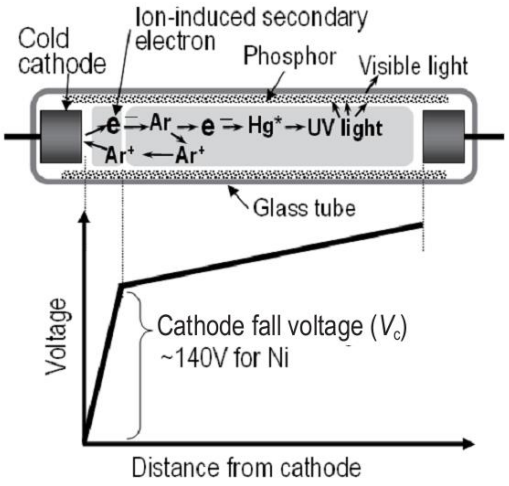

Figure 4. Diagram of a cold cathode fluorescent lamp showing cathode fall, V_C at increasing distance from the cathode [42]

1.3.3 – Secondary electron emission

Secondary emission refers to the emission of particles induced by incident particles with sufficient energy. Studies have been conducted using H terminated diamond films showing up to 20 times greater secondary electron emission (SEE) than presently used materials. [43] Unfortunately the diamond is unstable under continuous electron beam exposure, causing desorption of H and graphitisation of the diamond surface.

Mearini et al demonstrated secondary electron emission from CsI terminated diamond films which addresses the issues with H terminated films; no degradation of the material was seen after continuous electron beam exposure. The surface was very efficient, with secondary yield coefficients (σ) from 25 to 50. [43] Such a material could be used to build an electron amplifier with gain several orders of magnitude higher than currently available.

2.0 – Experimental

2.1 – Sample preparation

2.1.1 – Acid cleaning

Boron-doped CVD diamond samples were bought in and cut to size using a laser cutting system. They were then cleaned in 100 ml neat H_2SO_4 mixed with 6.5 g KNO_3.

2.1.2 – UVO cleaning

The Jelight UVO cleaning system utilises two different wavelengths of UV light. Light at 253.7 nm excites contaminant molecules on the surface being cleaned such as photoresist, resins, human skin oils, solvent residues and flux. Light at 184.9 nm converts O_2 from the air into molecular oxygen and O_3. O_3 is converted to molecular oxygen by light at 253.7 nm. The excited contaminant molecules react with the molecular oxygen to form simpler molecules that desorb from the surface and are pumped away, giving an atomically clean surface.

The molecular oxygen also oxidises a diamond surface at room temperature. This is important because diamond will graphitise and burn if heated above 500°C in an oxygen-containing atmosphere. [44] The acid-cleaned diamond samples were placed in the UVO cleaner for 30 minutes to clean the samples further and give an oxygen termination.

2.1.3 – Metal coating

Three oxygen-terminated diamond samples were placed onto glass slides and placed into a Baltzer 150 vacuum evaporation system. Under high vacuum, Mg was first degassed, and then heated to 700°C to evaporate it onto the samples. The process was repeated in a smaller vacuum evaporation system for Ti, Cr, Al and Ni, with the metals being heated to their respective boiling points.

2.1.4 – Acid washing

The glass slides coated with metal were used to test the metal's solubility in various concentrations of acid. Visible Mg was found to dissolve from the glass within 10m in 0.01M H_2SO_4 and 0.005M H_2SO_4. When left in water, the visible metal dissolved when left overnight. When the other metals were tested, it was found that heating was necessary to dissolve the metal in a reasonable amount of time. In all cases hereon, the acid used was HCl heated to 150°C. Table 2 shows the results of various acid concentrations for Ti, Cr, Al and Ni.

Metal	HCl concentration / M	Dissolves metal?	Time taken
Ti	12	Y	30m
	6	Y	30m
	3	Y	1h
	2	Y	1h
	1	N	N/A
Cr	12	Y	<1m
	6	Y	<1m
	4	Y	10m
	3	Y	15m
	2	Y	15m
	1	N	N/A
Al	12	Y	<1m
	6	Y	2m
	4	Y	3m
	3	Y	5m
	2	Y	5m
	1	Y	10m
	0.5	N	N/A
Ni	12	Y	<1m
	6	Y	1m
	4	Y	3m
	3	Y	5m
	2	Y	6m
	1	Y	8m
	0.5	Y	10m
	0.25	Y	20m
	0.125	N	N/A

Table 2. Experimental data for the length of time required to dissolve a thin film of metal from a glass slide at various concentrations of HCl.

It was decided to coat two CVD diamond samples with Mg, one on the smooth surface and one on the rough surface. These samples were both sonicated in 0.005 H_2SO_4 for 15m. Based on the results of this, it was decided to only coat the smooth diamond surface in future.

Concentrations and durations of washing for the CVD diamond samples were based on the weakest acid that dissolved the metal, in order to increase the likelihood of leaving a monolayer on the diamond surface rather than removing all traces of the metal. Two of the three coated samples for each metal were washed, with the third left unwashed for comparison. Table 3 details the concentrations and timings of the washes used on the CVD diamond samples.

Sample	[HCl] / M	Time washed / minutes
Ti 1	2	60
Ti 2	4	30
Cr 1	2	15
Cr 2	3	15
Al 1	1	10
Al 2	0.5	20
Ni 1	0.5	10
Ni 2	0.25	20

Table 3. Acid concentrations and durations of washing used for each CVD diamond sample.

2.2 – Sample analysis

2.2.1 – Scanning electron microscopy (SEM)

A Jeol JSM-5600LV SEM was used extensively to examine the coated and washed CVD diamond surfaces, as well as provide an indication of their NEA based on sample brightness due to electron emission. SEM is capable of magnification up to 500,000 times, far beyond the limits of optical microscopy, which can only magnify up to 2000 times. The technique involves scanning an electron beam over the surface of the sample and detecting the electrons scattered by and emitted from the surface.

The primary electrons are generated by an electron gun fitted with a tungsten filament cathode situated above the sample. The gun in the instrument used operates at voltages between 0 and 30 keV. The electrons are focussed into a beam by lenses, which then travels through a pair of scan coils which can deflect the beam in the x and y direction. This allows scanning of a rectangular area on the sample surface. The secondary electrons emitted from the surface are analysed by a collector, which generates an image on screen. The image appears sharp and deep due to the number of secondary electrons emitted from the surface. The whole process is carried out under high vacuum. Figure 5 depicts an SEM.

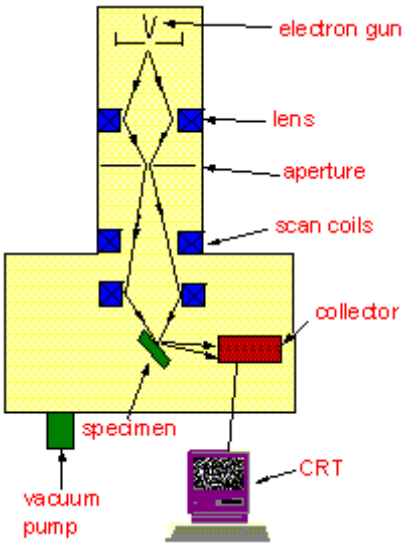

Figure 5. Schematic diagram of an SEM instrument. [45]

2.2.2 – Energy-dispersive X-ray spectroscopy (EDX)

EDX was used to examine the surface composition of each diamond sample and qualitatively determine which elements were present. EDX involves firing an electron beam at the sample and measuring the number and energy of emitted X-rays. The electron beam is from the SEM and the detector is an Oxford Instruments ISIS 300 system. These X-rays arise from ground-state electrons in low-energy shells being excited by the electron beam and leaving holes behind. Electrons from high-energy shells move to fill the holes, causing characteristic X-ray emission for each element. This allows the elemental composition of the sample to be examined.

2.2.3 – Atomic force microscopy (AFM)

AFM was used to examine the glass slides the diamond samples were placed on during the coating process, thus giving the thickness of the metal layer on the unwashed samples. AFM uses a cantilever with a sharp tip that is scanned across the sample surface. The tip is deflected in response to the surface composition. Laser light is reflected off the cantilever onto a split photodiode detector, which gives a picture of the surface down to the atomic scale. There would be a risk of damage to the tip if it were scanned at a constant height, so the sample is mounted on a piezoelectric tube which moves up and down to maintain a constant force between the tip and the sample. Figure 6 shows a diagram of an AFM instrument.

The instrument used was a Veeco Multimode V with Nanoscope 3D controller in contact mode, scan size 40 μm x 40 μm, resolution 512 x 512, scanning at 3.95 Hz, which equates to a 20 μm s^{-1} tip velocity. The tip used was a Silicon Nitride 20 μm tip.

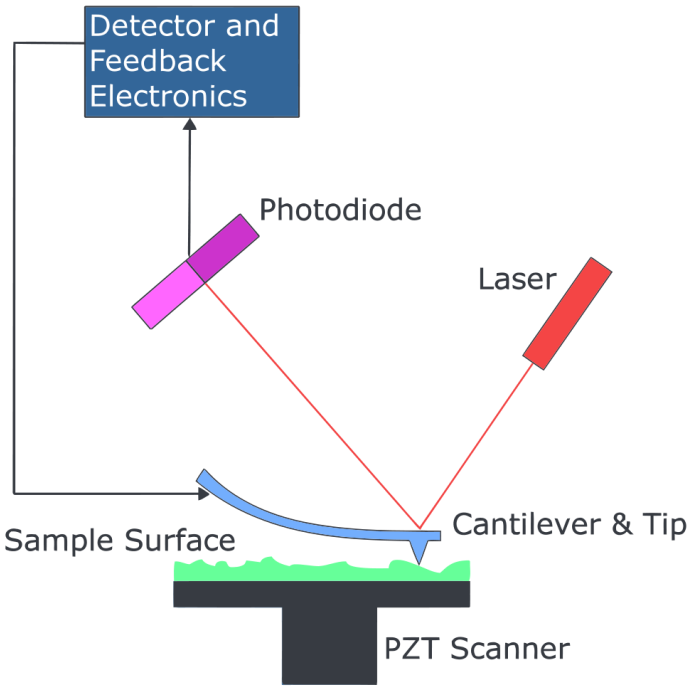

Figure 6. Schematic diagram of an AFM instrument.

2.2.4 – Raman spectroscopy

Raman spectroscopy was used to help characterise the metal films deposited on the diamond surfaces. The technique is used to study vibrational and rotational modes in a system by analysing the inelastic scattering of monochromatic light. A laser is shone at the sample, and the scattered light is fed through a notch filter that removes light close in wavelength to the laser. The remaining light is analysed by a detector, which generates the spectrum. The light that is filtered out is the result of Rayleigh scattering, or elastic scattering of light. The remaining light is the result of Raman scattering, or inelastic scattering of light. This light has either higher (anti-Stokes) or lower (Stokes) frequency than the incident light. This is shown in figure 7. The shift in frequency gives chemical information about the sample.

The anti-Stokes band is much less intense than the Stokes band because thermal population of $v = 1$ is much lower than $v = 0$ as modelled by the Boltzmann distribution. Raman scattering is also far less probable than Rayleigh scattering. This limits the usefulness of Raman spectroscopy as an analytical tool as the signal is very weak.

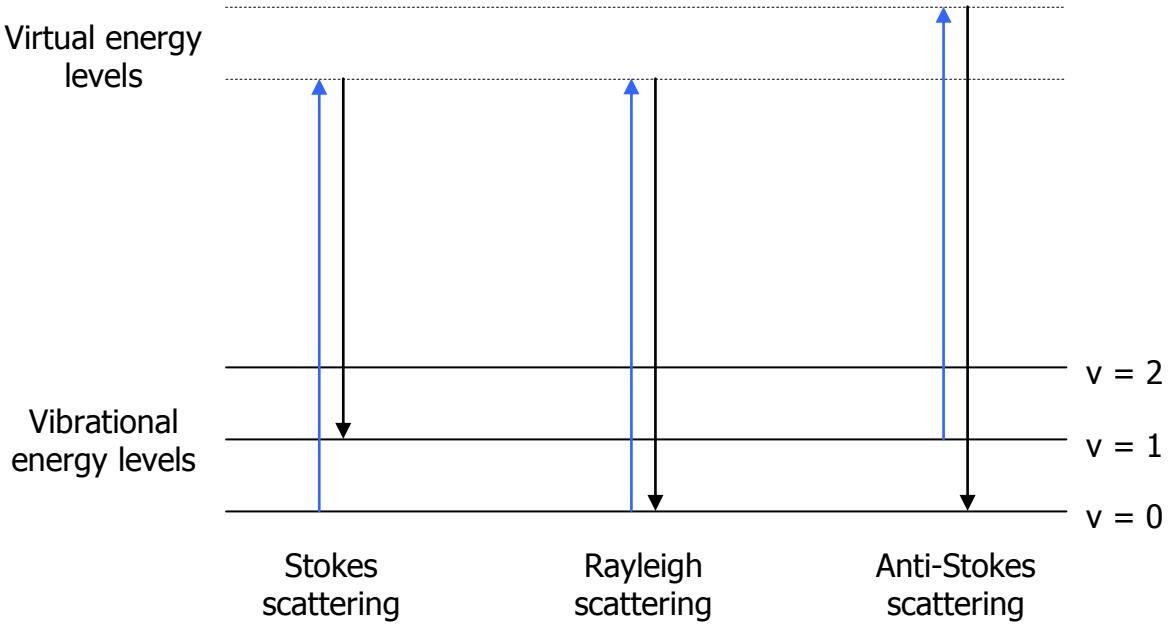

Figure 7. Diagram showing Rayleigh and Raman scattering of light.

2.2.5 – Conductivity measurements

Conductivity measurements of the samples were carried out using a basic 2-point probe on opposite corners of the sample, as shown in figure 8.

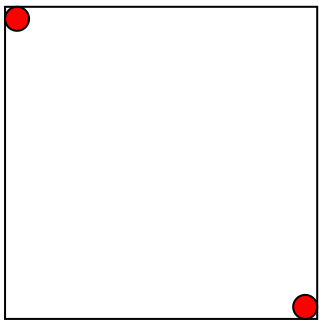

Figure 8. Diagram showing the contact points (red circles) of the 2-point probe used on the diamond samples.

3.0 – Results and discussion

3.1 – Surface morphology and composition

Clean H-terminated and O-terminated diamond surfaces were examined with the SEM to provide a comparison for the metal-coated surfaces and to demonstrate that surfaces with NEA appear bright in the image due to secondary electron emission, as seen in figure 9.

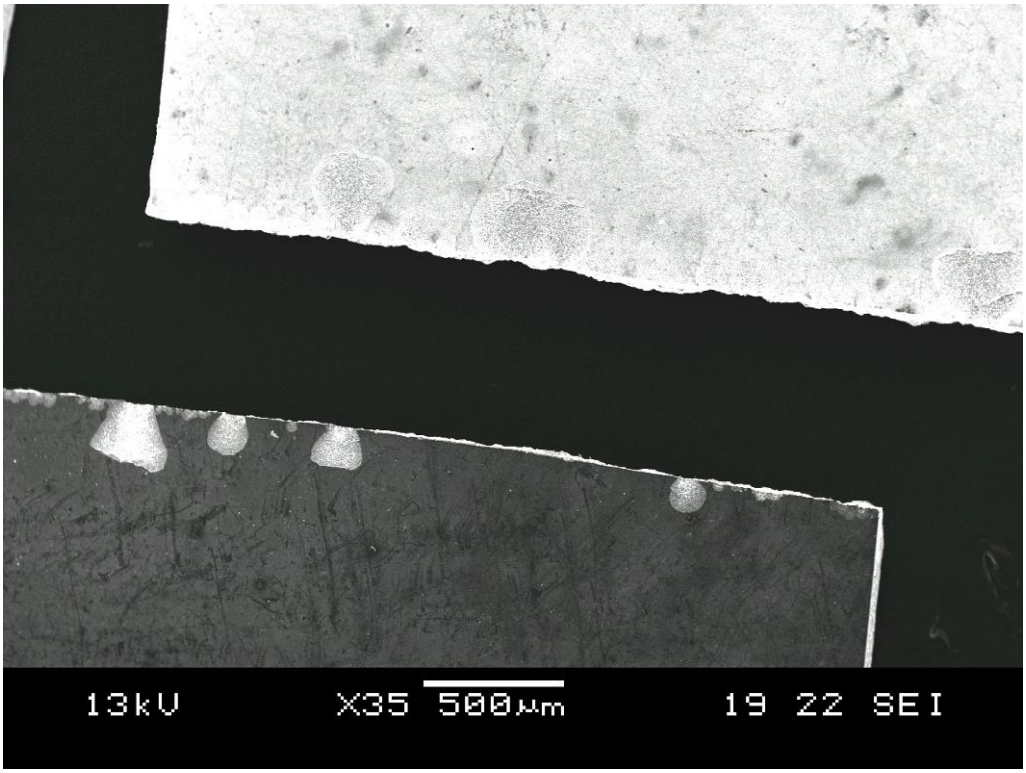

Figure 9. SEM of H-terminated diamond surface (top) and O-terminated surface (bottom). It can clearly be seen that the H-terminated surface is brighter due to its NEA.

EDX analysis was performed on the O-terminated surface. The only elements detected were C and O, consistent with a diamond surface terminated with O. This is shown in figure 10.

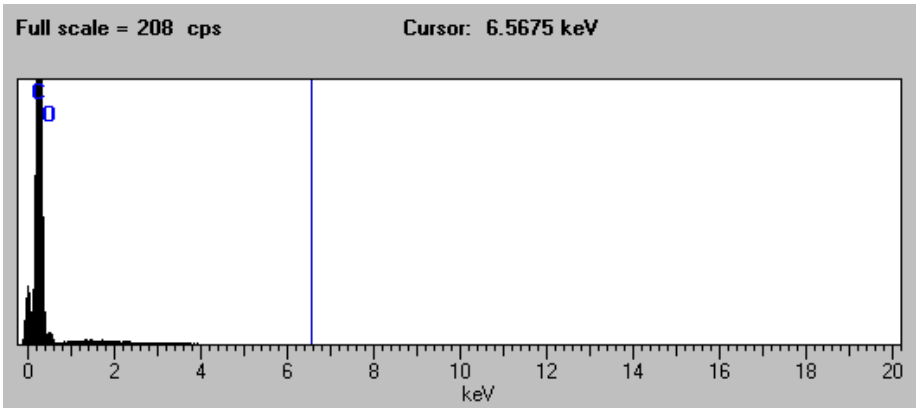

Figure 10. EDX of O-terminated diamond surface, showing only the presence of C and O.

3.1.1 – Magnesium coating

Glass coated with Mg was examined with SEM and EDX to investigate the surface morphology and composition before and after washing with water, 0.01M H_2SO_4 and 0.005M H_2SO_4. The EDX analyses shown in figures 11-14 show the amount of Mg present decreasing with increasing wash concentration. The SEM images show crystals of deposited metal in figure 15, and the results of the various washes can be seen in figures 16-18. 0.005M H_2SO_4 seems to give the smoothest, most homogeneous surface.

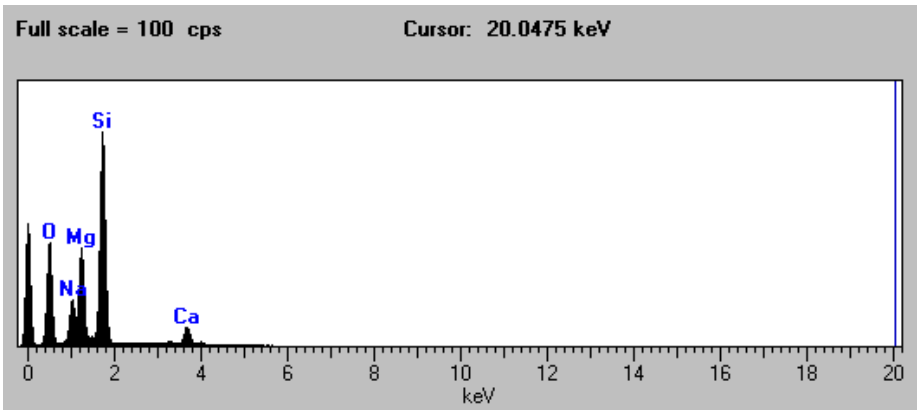

Figure 11. EDX of Mg deposited on glass. Si, O and Mg are the main peaks, as well as Ca and Na due to the composition of glass.

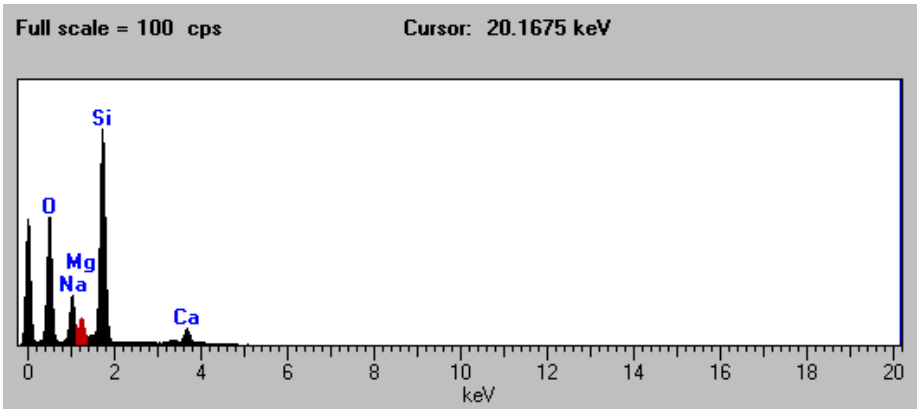

Figure 12. EDX of Mg deposited on glass washed with water. It can be seen that the peak for Mg has decreased in intensity significantly compared with the unwashed sample.

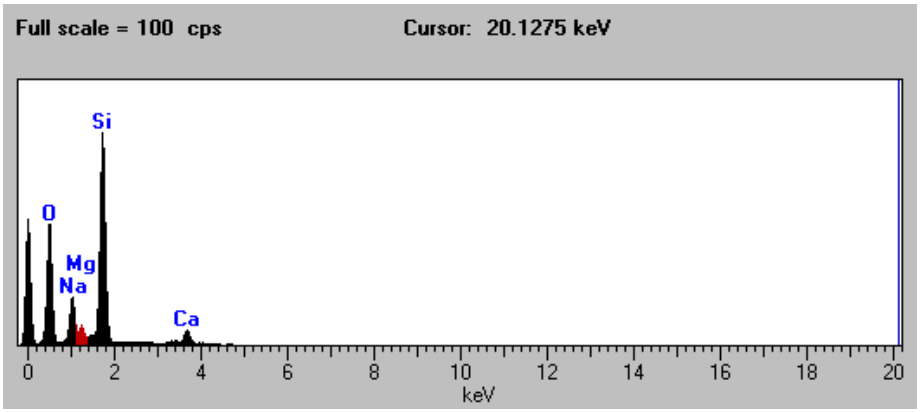

Figure 13. EDX of Mg deposited on glass washed with 0.005M H_2SO_4. It can be seen that the peak for Mg has decreased further compared with the sample washed in water.

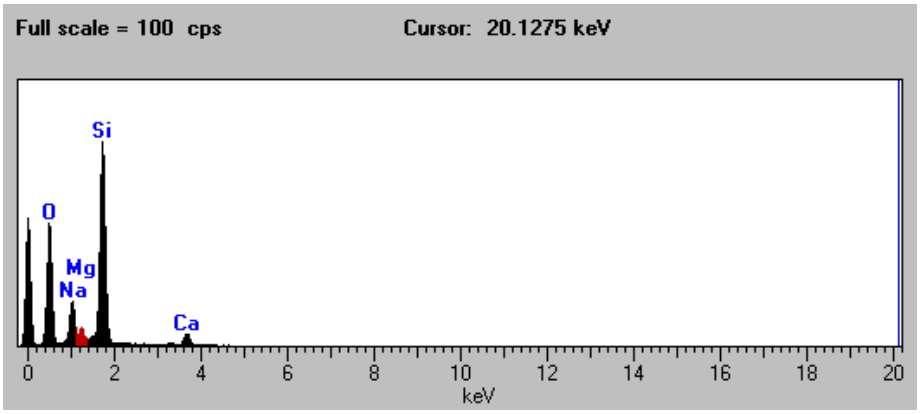

Figure 14. EDX of Mg deposited on glass washed with 0.01M H_2SO_4. It can be seen that the peak for Mg has decreased even further compared with the sample washed in water.

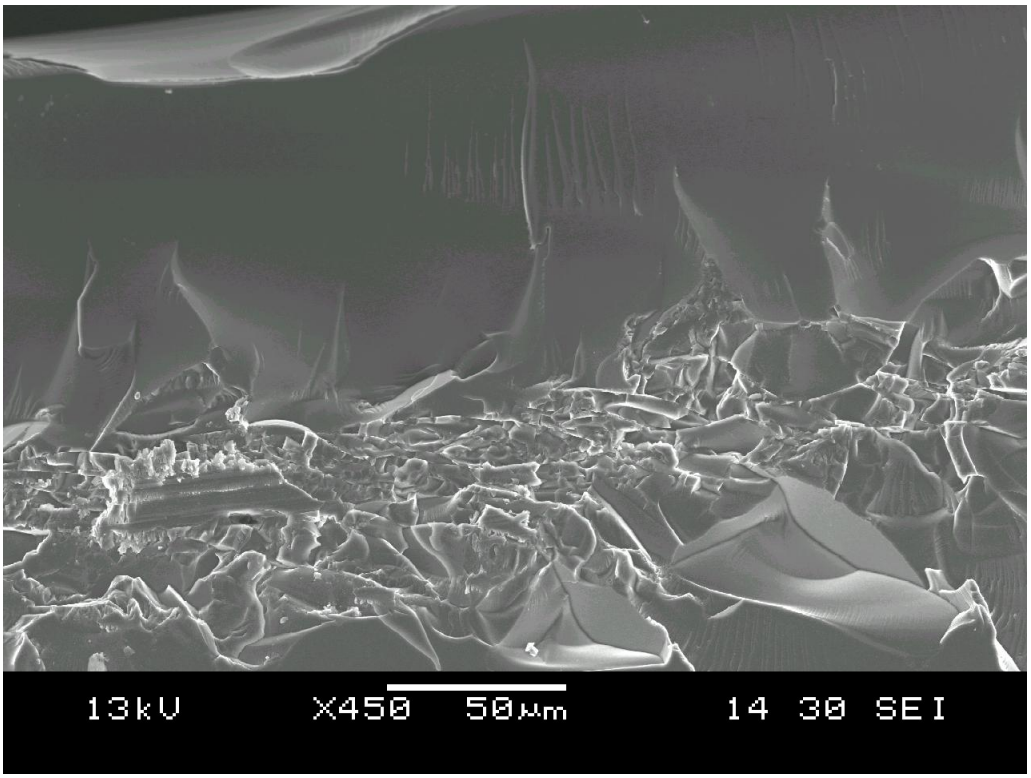

Figure 15. SEM of Mg deposited on glass, showing crystals of metal.

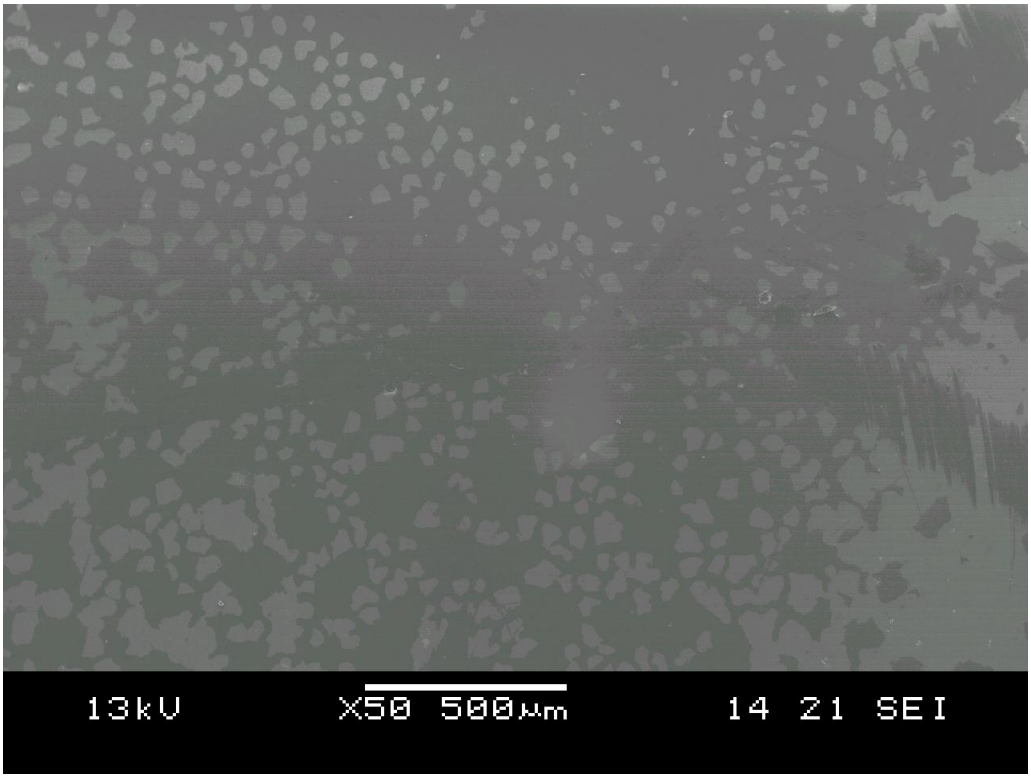

Figure 16. SEM of Mg on glass washed with water. Crystals of metal seem undissolved, implying that the wash was too weak.

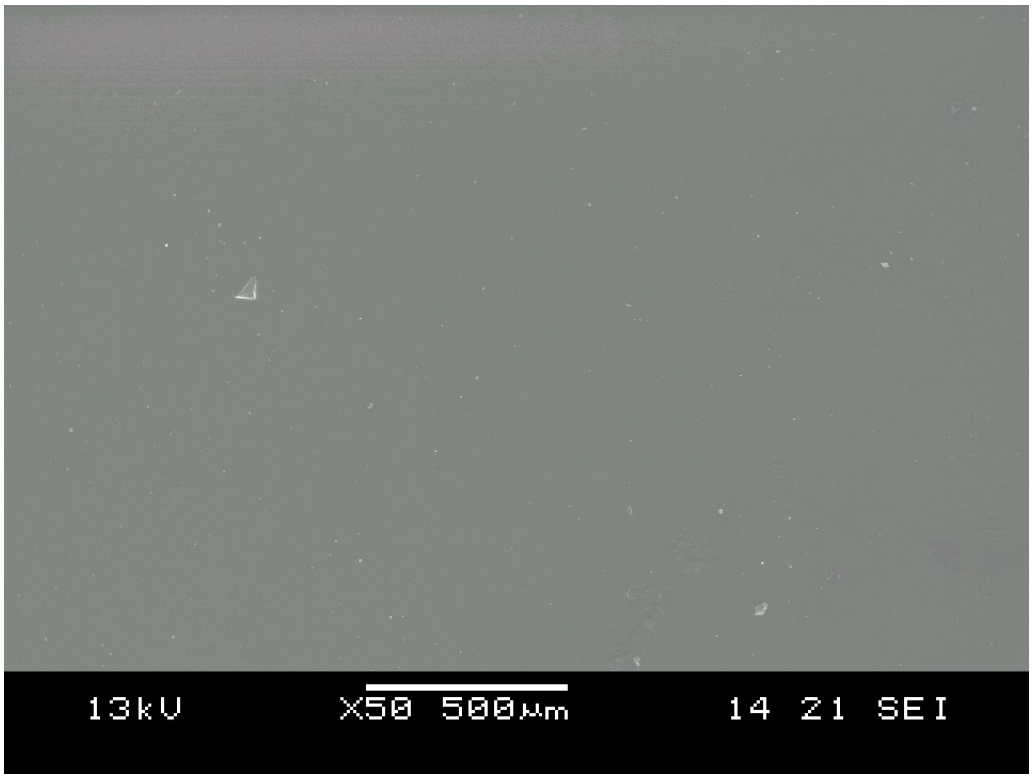

Figure 17. SEM of Mg on glass washed with 0.005M H_2SO_4. The surface seems very homogeneous and smooth.

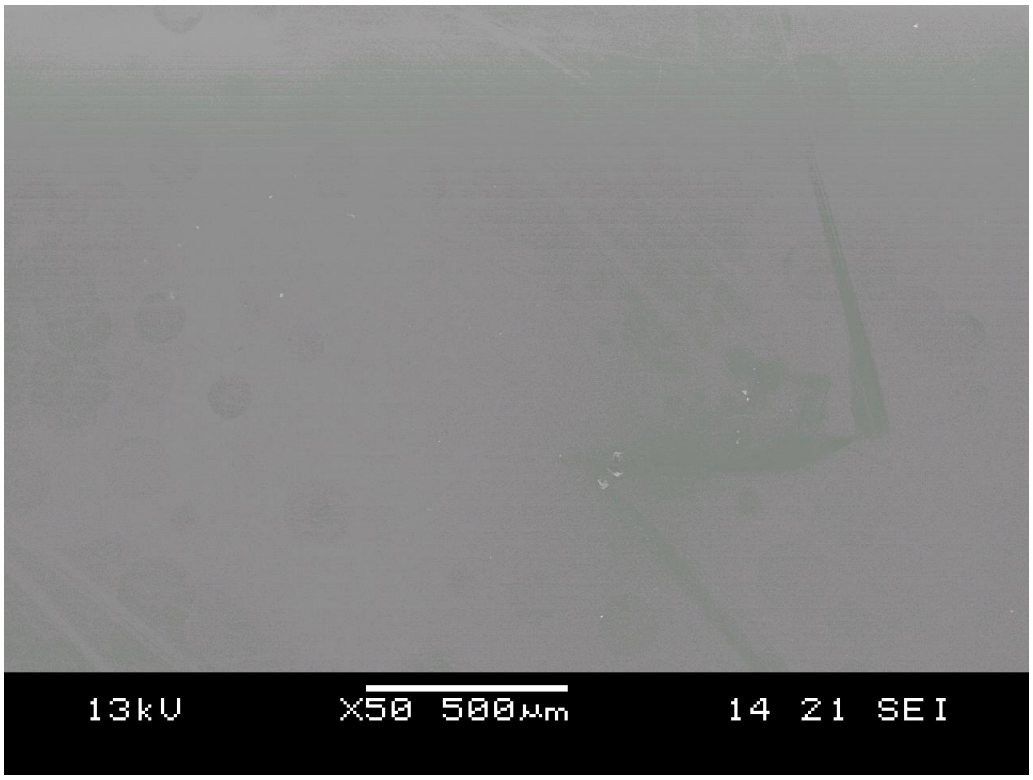

Figure 18. SEM of Mg on glass washed with 0.01M H_2SO_4. The surface seems fairly homogeneous.

The two CVD diamond samples coated with Mg and washed in 0.005M H_2SO_4 were analysed. The rough side of the diamond makes it hard to tell if the surface is smooth and homogeneous, so it was decided to use only the smooth side for the other metal coatings. The EDX analysis showed the presence of magnesium on both samples. See figures 19 and 20 for EDX data and figures 21 and 22 for SEM images.

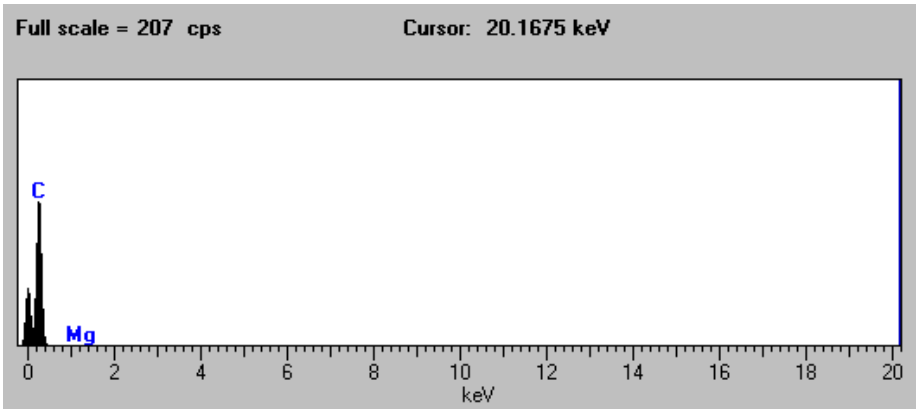

Figure 19. EDX of Mg deposited on smooth CVD diamond surface and washed with 0.005M H_2SO_4. A small trace of magnesium is present.

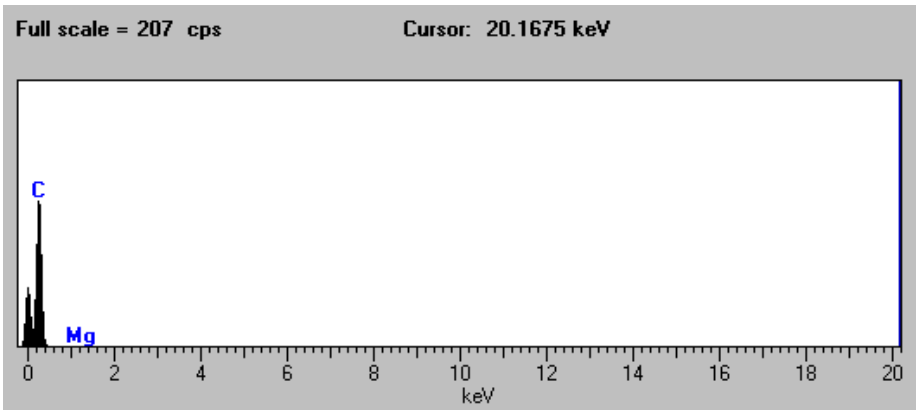

Figure 20. EDX of Mg deposited on rough CVD diamond surface and washed with 0.005M H_2SO_4. A small trace of magnesium is present.

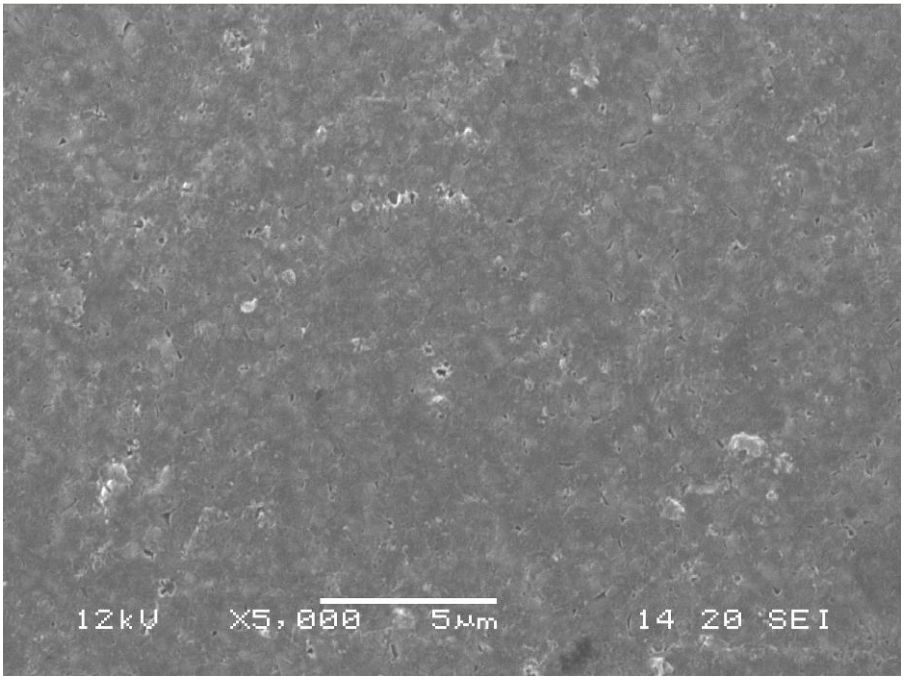

Figure 21. SEM of Mg deposited on smooth CVD diamond surface and washed with 0.005M H_2SO_4. The surface appears fairly clean and homogeneous.

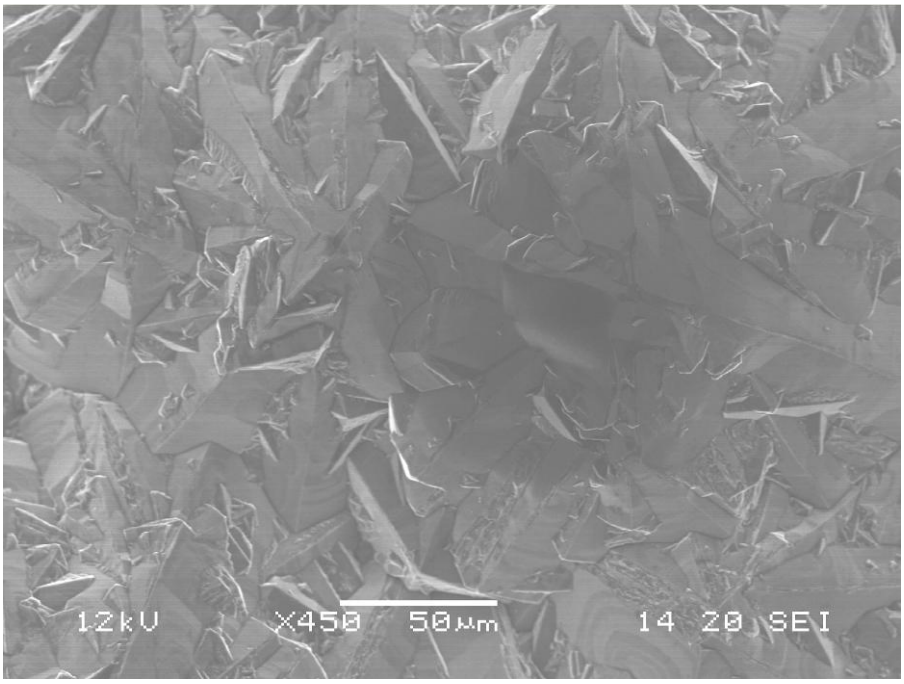

Figure 22. SEM of Mg deposited on rough CVD diamond surface and washed with 0.005M H_2SO_4. The surface appears clean, but it is hard to tell if the coating is homogeneous or if crystals of Mg are present.

3.1.2 – Titanium coating

The Ti coated samples showed fairly smooth, homogenous surfaces at both 2M and 4M wash concentrations. The 2M washed surface appears brighter when compared with the unwashed surface, as shown in figure 23.

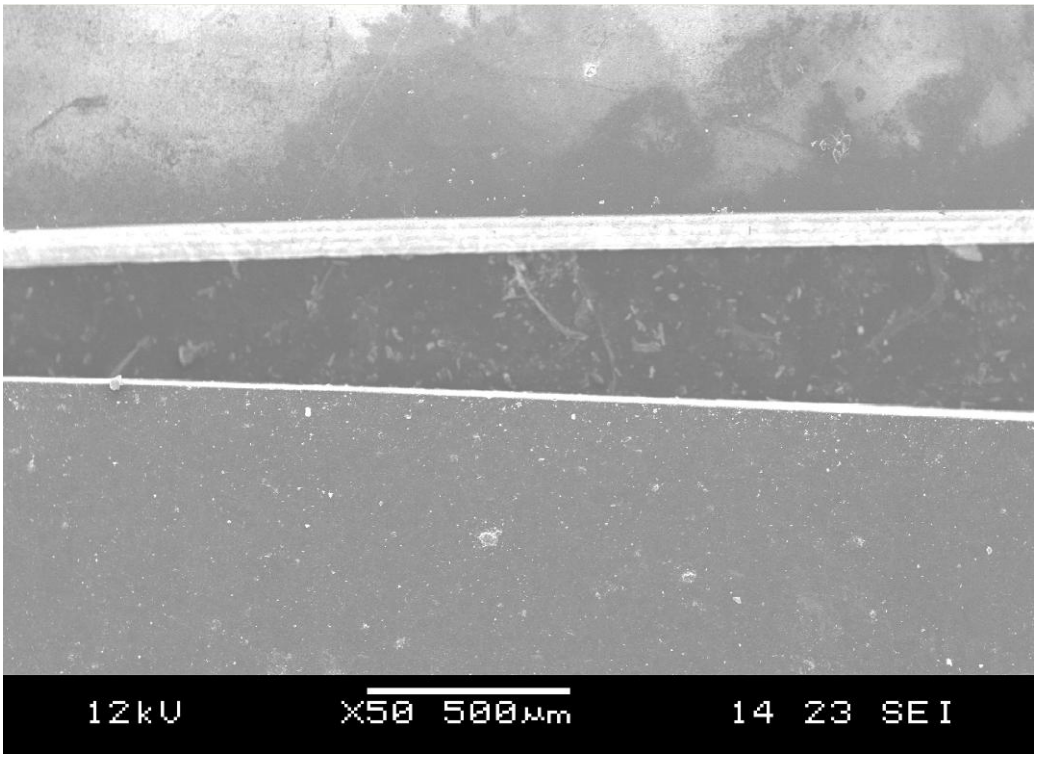

Figure 23. SEM of Ti coated diamond sample unwashed (bottom) and washed in 2M HCl (top). The washed surface appears brighter, indicating NEA at the surface.

Analysis of EDX data reveals the presence of Ti on the unwashed surface, but no evidence to suggest presence on either of the washed surfaces. This could indicate either that all the metal has been washed away, or that EDX is not sensitive enough to detect a monolayer at the surface. For this and all other data not included in this section, see Appendix 7.1 and 7.2.

3.1.3 – Chromium coating

The Cr coated samples all showed very smooth, homogeneous surfaces. The three are shown side by side in figure 24. The sample washed in 3M H_2SO_4 appears the brightest, indicative of NEA at the surface. Analysis of EDX data shows the presence of Cr on all three surfaces, decreasing in intensity from unwashed to washed in 2M to washed in 3M. This implies that 3M has the thinnest layer of metal.

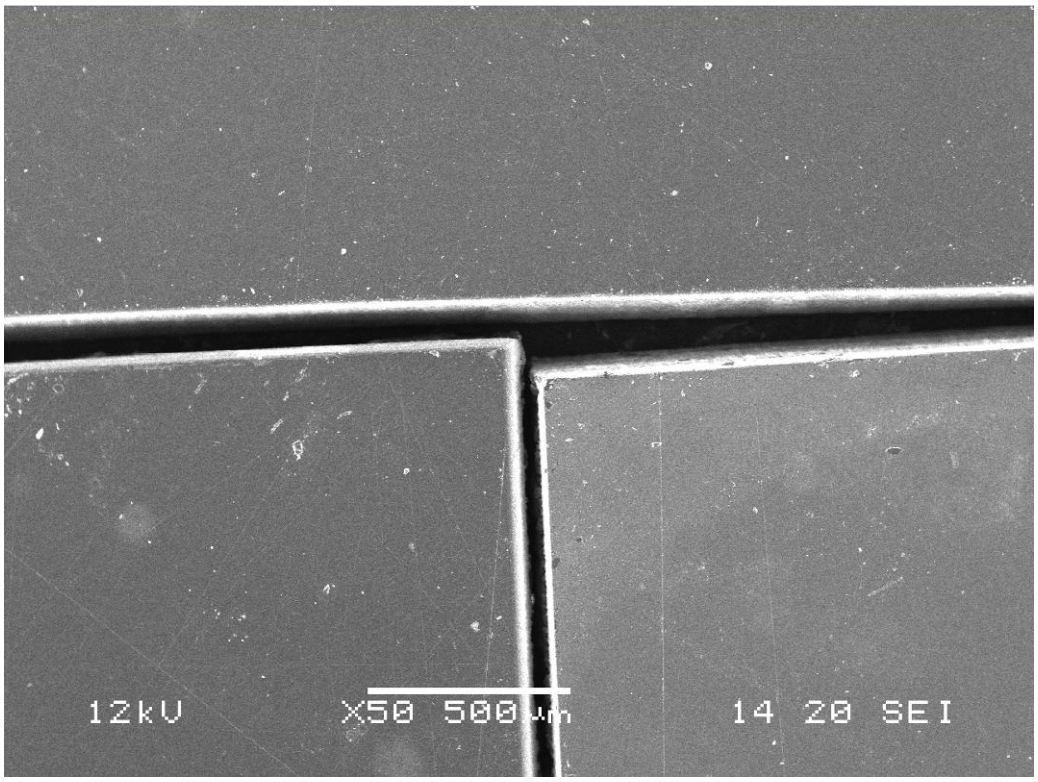

Figure 24. SEM of Cr coated diamond sample unwashed (top), washed in 2M H_2SO_4 (left) and washed in 3M H_2SO_4 (right). The surface washed in 3M H_2SO_4 appears brightest, indicating NEA at the surface.

3.1.4 – Aluminium coating

The Al coated samples all showed reasonably smooth, homogeneous surfaces. The three are shown side by side in figure 25. The sample washed in 0.5M H_2SO_4 appears the brightest, indicative of NEA at the surface. Analysis of EDX data shows the presence of Al on the unwashed surface but no evidence to suggest presence on either of the washed surfaces, as with Ti. This could indicate either that all the metal has been washed away, or that EDX is not sensitive enough to detect a monolayer at the surface.

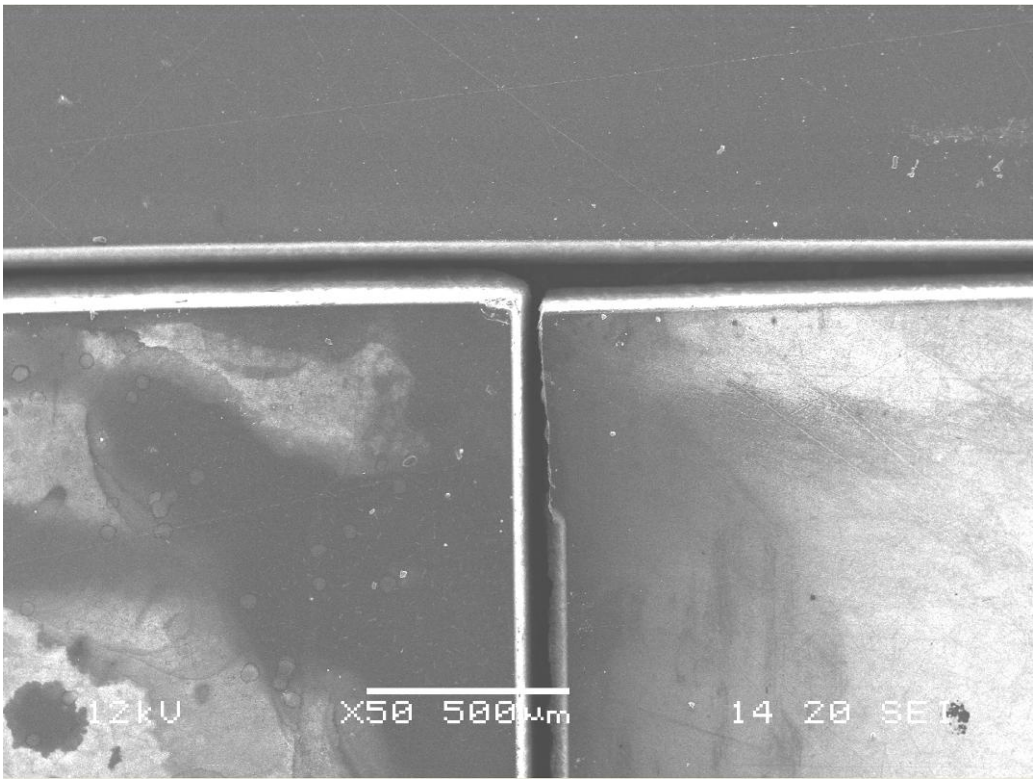
12kV
X50 500µm
14 20 SE

Figure 25. SEM of Al coated diamond sample unwashed (top), washed in 1M H_2SO_4 (left) and washed in 0.5M H_2SO_4 (right). The surface washed in 0.5 H_2SO_4 appears brightest, indicating NEA at the surface.

3.1.5 – Nickel coating

The Ni coated samples all showed reasonably smooth, homogeneous surfaces. The three are shown side by side in figure 26. The sample washed in 0.5M H_2SO_4 appears the brightest by far, indicative of NEA at the surface. Analysis of EDX data shows the presence of Al on the unwashed surface, and a reduced amount present on the 0.25M washed surface. The 0.5M washed surface does not show any evidence of Ni on the surface. As before, this could indicate either that all the metal has been washed away, or that EDX is not sensitive enough to detect a monolayer at the surface.

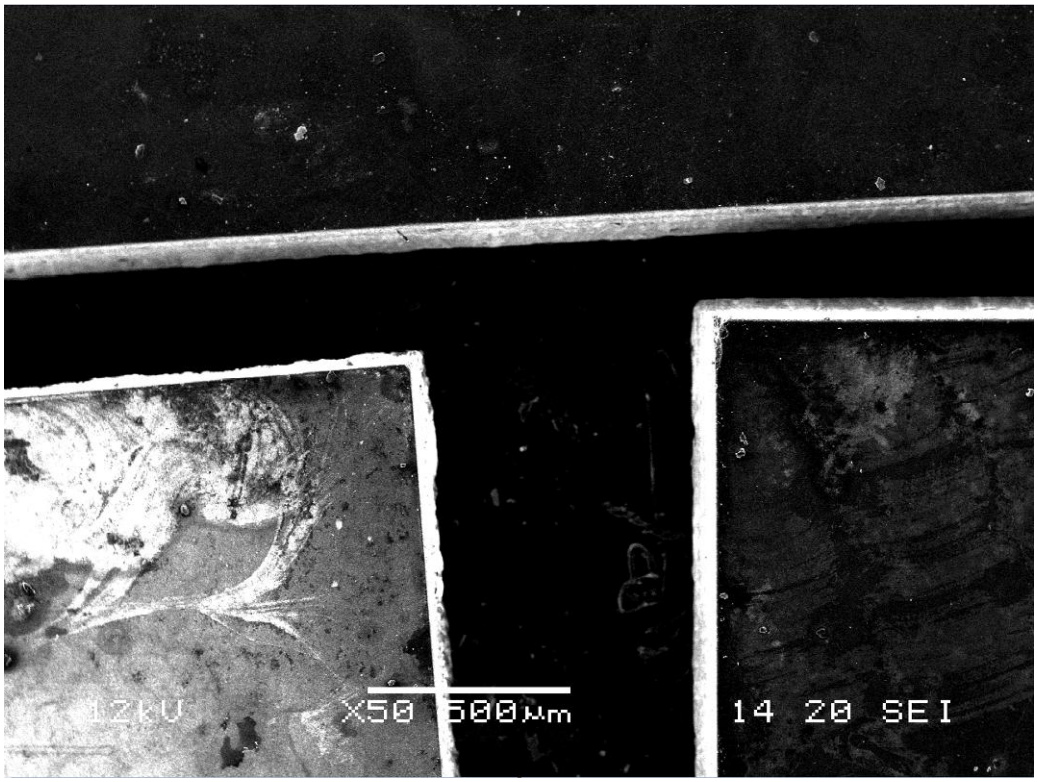

Figure 26. SEM of Ni coated diamond sample unwashed (top), washed in 0.5M H_2SO_4 (left) and washed in 0.25M H_2SO_4 (right). The surface washed in 0.5M H_2SO_4 appears brightest, indicating NEA at the surface.

3.2 – Raman results

Raman spectroscopy is an excellent tool for characterising diamond samples, as diamond shows a large peak at 1332 cm^{-1} due to the presence of sp^3 hybridised C atoms. [46] All the samples were analysed using a UV laser Raman system. Figure 27 shows the Raman spectra for the three Al samples. The unwashed sample does not show any particular peaks, indicating that the diamond surface is covered by a layer of metal. The sample washed in 0.5M HCl shows a small peak at 1332 cm^{-1}, indicating that the diamond surface is partially exposed. The sample washed in 1M HCl shows a large peak at 1332 cm^{-1}, indicating that there is a thin layer of metal on the surface, or none at all.

The spectra for the other metals tell a similar story, except in the case of Cr, where all three spectra are just noise. This indicates that there is a thick layer of metal on all three samples, despite acid washing. These spectra can be found in Appendix 7.3.

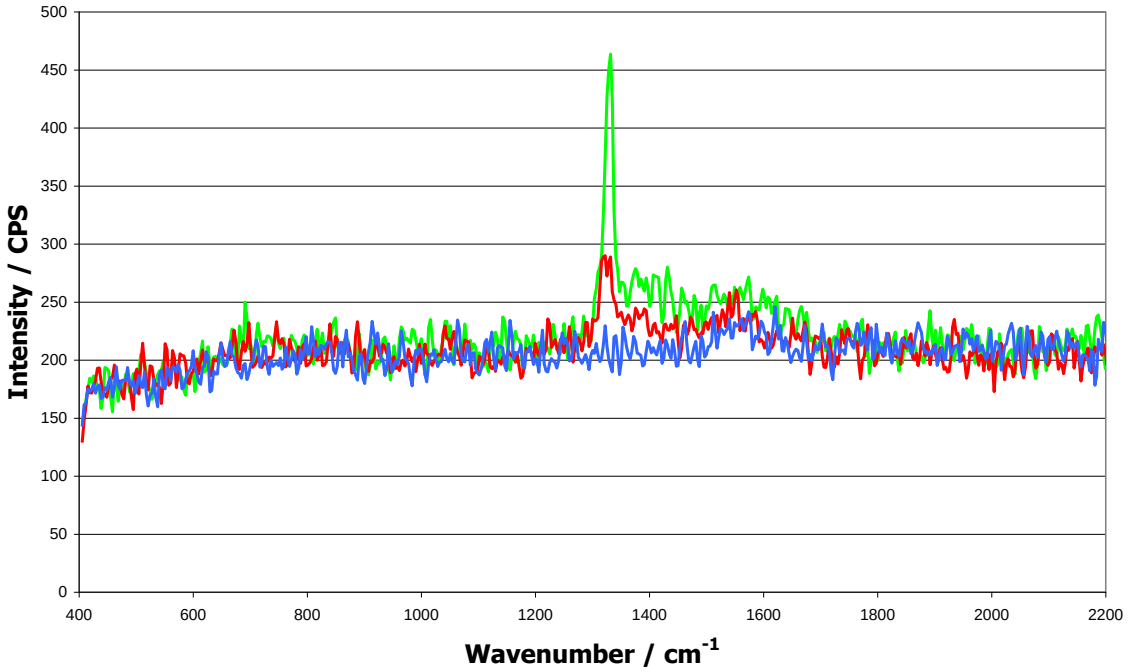

Figure 27. Raman spectra of Al coated diamond samples; unwashed in blue, washed in 0.5M HCl in red and washed in 1M HCl in green.

3.3 – AFM results

For Ti and Cr, the metal coating was thick enough to obtain a figure for the thickness from the AFM data. Figure 28 shows AFM data for Cr. By calculating values from the two equations at equivalent y, a thickness of 96.7 nm is obtained. For Ti, the thickness is calculated to be 42.4 nm.

For Al and Ni, the coating was too thin to obtain precise enough data to calculate the thickness. 3D and 2D images of each sample were generated to show the boundary of the metal and the clean glass surface, for example Al as shown in figure 29. The 2D images of Al and Ni reveal a pattern of raised dots, presumably metal sputtered onto the sample. The other images can be found in Appendix 7.4.

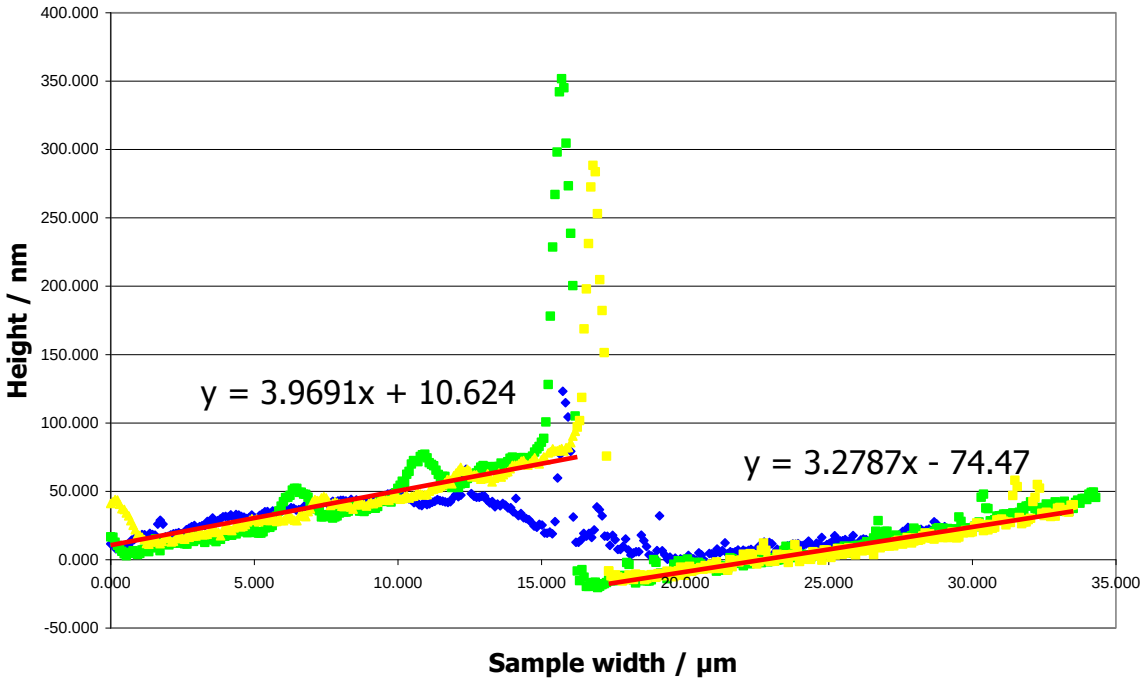

Figure 28. AFM data for Cr with equations to calculate the step size of metal and hence the thickness of the coating on the diamond samples.

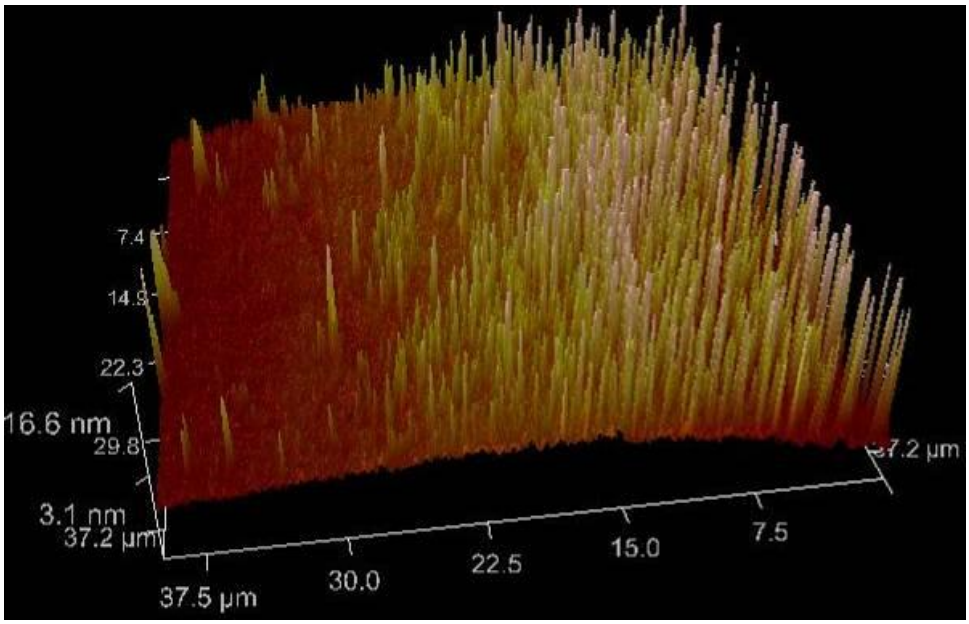

Figure 29. AFM data for Al represented in 3D, showing the edge of the metal and the clean glass surface. The metal is shown by the spikes on the image.

3.4 – Conductivity results

The conductivity of each sample was measured using a 2-point probe. This only provides preliminary data; a 4-point probe would be required to give more reliable data. The results are shown in table 4.

Sample	Resistance / Ω
H-terminated diamond	8.3
Mg rough washed in 0.005 H_2SO_4	24.4
Mg smooth washed in 0.005 H_2SO_4	9.3
Ti unwashed	15.3
Ti washed in 2M HCl	12.5
Ti washed in 4M HCl	8.1
Cr unwashed	13.6
Cr washed in 2M HCl	10.0
Cr washed in 3M HCl	9.1
Al unwashed	7.0
Al washed in 0.5M HCl	8.1
Al washed in 1M HCl	12.1
Ni unwashed	8.9
Ni washed in 0.25M HCl	14.4
Ni washed in 0.5M HCl	13.5

These results show resistance decreasing for Ti and Cr as the metal is washed away, whereas it increases for Al and Ni as the metal is washed away. This is consistent with Al and Ni being better conductors than Cr and Ti.

4.0 – Conclusions

CVD diamond samples were coated with metals and the excess removed with varying degrees of success. The Cr coated samples had a layer of metal that was ~100 nm thick, as shown the AFM data. The acid washes did not remove enough material as shown by the Raman and EDX data, and only a hint of NEA was observed. The three samples all appeared very similar under the SEM in terms of smoothness.

The Ti coated samples washed in HCl did not show any signs of Ti in the EDX data, and the Raman and conductivity data are inconclusive in terms of establishing if a monolayer of metal is present. The sample washed in 2M HCl looks the most promising in terms of NEA, although this could be the clean O-terminated surface if all the Ti was dissolved during the acid wash.

The Al coated samples similarly did not show any signs of Al in the EDX data, and the Raman and conductivity data are also inconclusive. The sample washed in 0.5M HCl is the most promising in terms of NEA, but as above, this could just be the clean O-terminated surface.

The Ni coated samples were the most promising. The sample washed in 0.25M HCl showed signs of Ni in the EDX data but the sample washed in 0.5M HCl did not. This sample was very bright in the SEM images, but as above, this could just be the clean O-terminated surface. However, the Raman data suggests that the two washed surfaces are very similar in composition as the peaks at 1332 cm^{-1} are almost the same height. Based on the data I have available, I conclude that the Ni diamond sample washed in 0.5M HCl is the closest I have come to depositing a monolayer of metal on a surface, and it appears to induce NEA at the surface.

5.0 – Future work

It is clear that a different analysis method is required to accurately determine if a monolayer of metal is present at the surface. Secondary ion mass spectrometry (SIMS) would be ideal for this, as it returns a depth profile of a thin film, allowing measurement of the thickness of a monolayer, if present. The acid wash concentrations and exposure times could then be fine-tuned so that a monolayer of metal is left on the diamond surface.

NiO appears to impart NEA at a diamond surface, so this could be studied further, for example obtaining a value for the NEA and comparing with other surface terminations. There is also some evidence to suggest that AlO and TiO impart NEA at a diamond surface, so this could be studied further as above.

The smoothness of the coatings could be improved by depositing a thicker layer of metal initially, and a stronger/longer acid wash to remove the excess. This would give a more uniform layer as was seen with the Cr coatings. A coating thickness of 100 nm should be aimed for.

6.0 – Acknowledgements

I would like to thank Prof. Paul May and Dr. Neil Fox for their help and guidance during my research, Zamir Othman for showing me how to use the instruments in the diamond lab and providing general advice, James Smith for assisting me in operating the metal evaporating system and Benoit Quignon for assisting me in obtaining the AFM data.

7.0 – Appendix

7.1 – SEM data

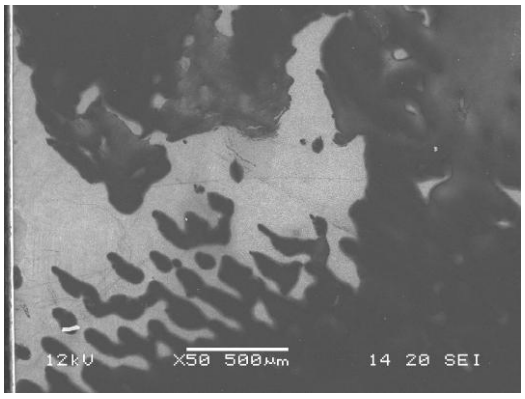

Figure 7.1.1. Smooth surface coated with Mg and washed in 0.005M H_2SO_4

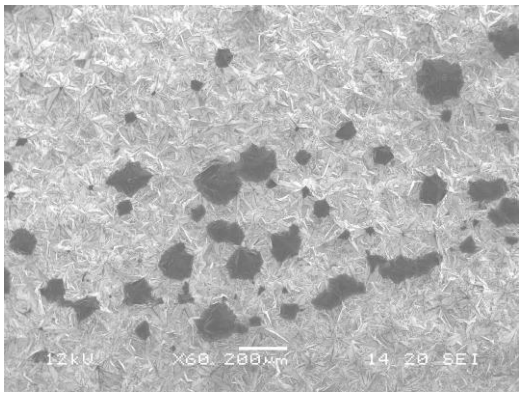

Figure 7.1.2. Rough surface coated with Mg and washed in 0.005M H_2SO_4

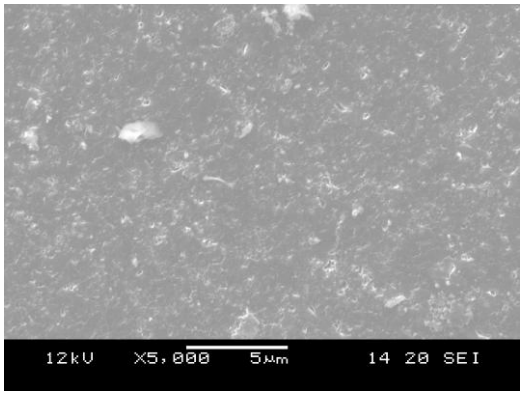

Figure 7.1.3. Unwashed Ti coated surface

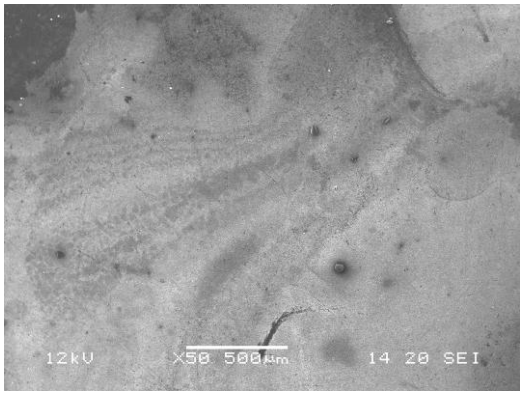

Figure 7.1.4. Ti coated surface washed in 2M HCl

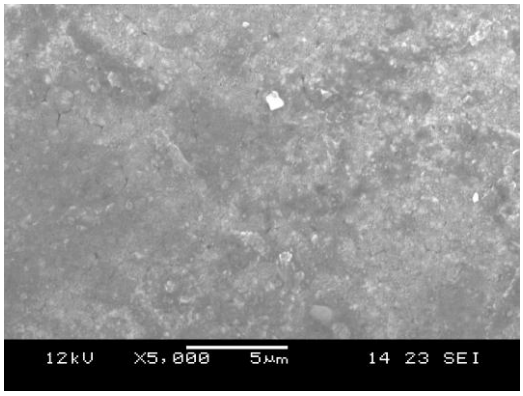

Figure 7.1.5. Ti coated surface washed in 2M HCl

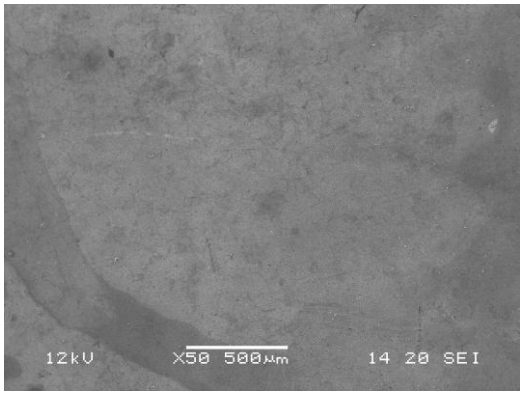

Figure 7.1.6. Ti coated surface washed in 4M HCl

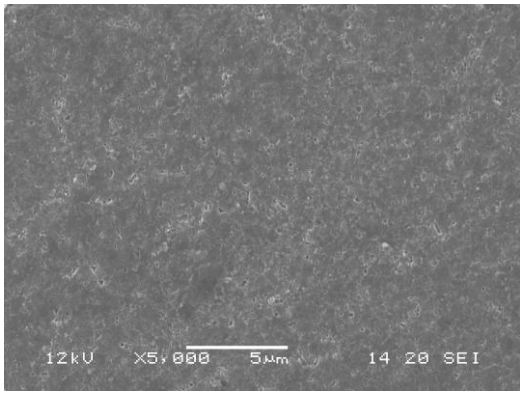

Figure 7.1.7. Ti coated surface washed in 4M HCl

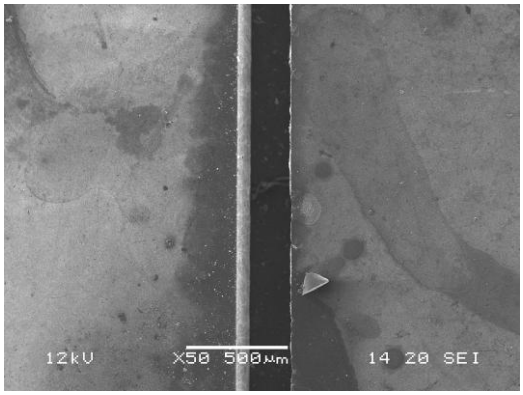

Figure 7.1.8. Ti coated surface washed in 2M HCl (left) and 4M HCl (right)

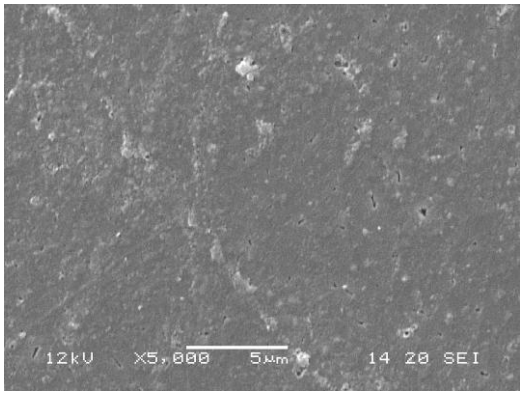

Figure 7.1.9. Unwashed Cr coated surface

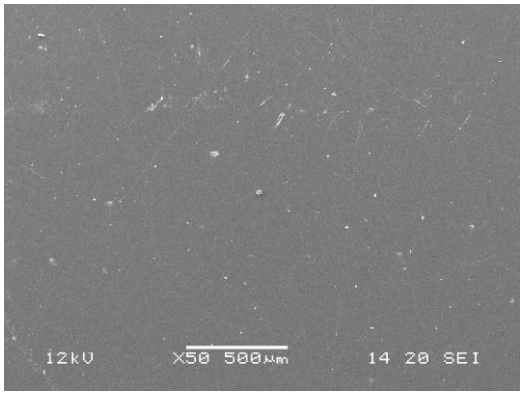

Figure 7.1.10. Unwashed Cr coated surface

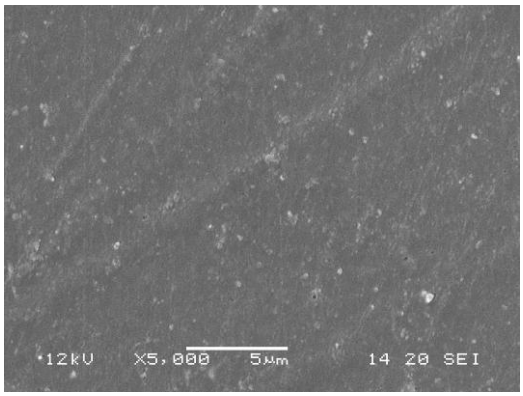

Figure 7.1.11. Cr coated surface washed in 2M HCl

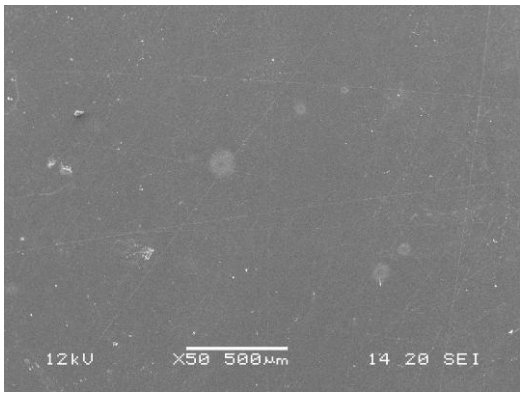

Figure 7.1.12. Cr coated surface washed in 2M HCl

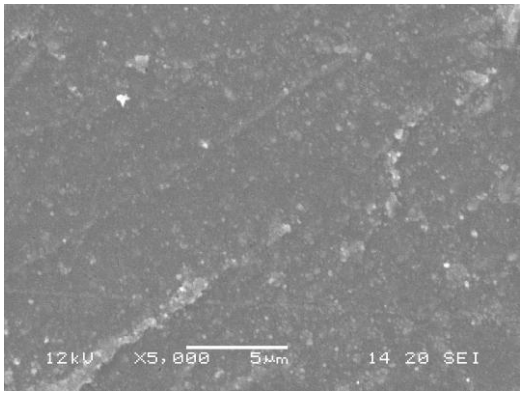

Figure 7.1.13. Cr coated surface washed in 3M HCl

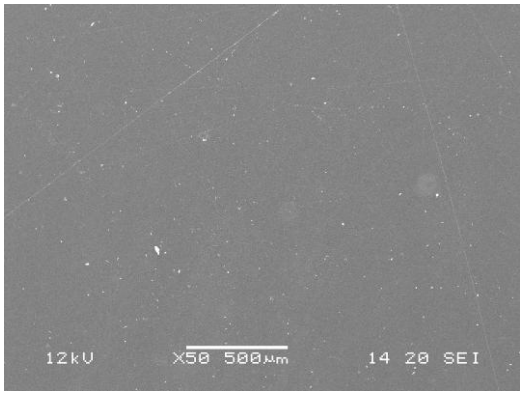

Figure 7.1.14. Cr coated surface washed in 3M HCl

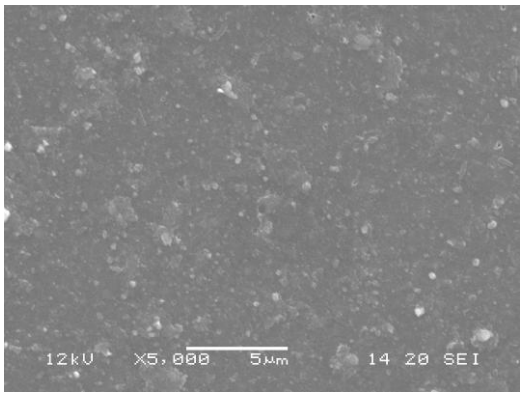

Figure 7.1.15. Unwashed Al coated surface

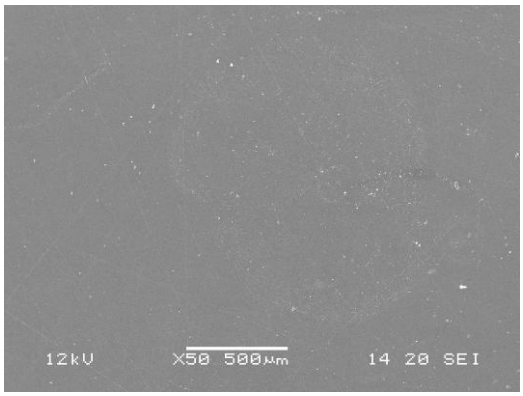

Figure 7.1.16. Unwashed Al coated surface

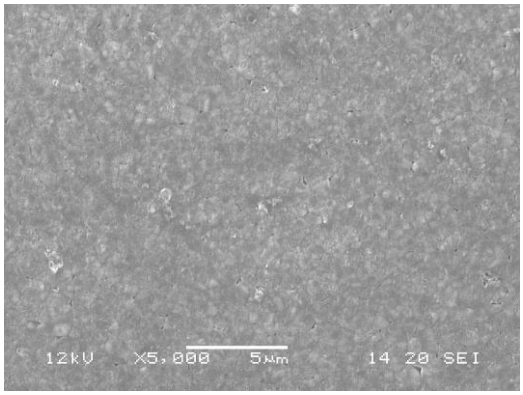

Figure 7.1.17. Al coated surface washed in 0.5M HCl

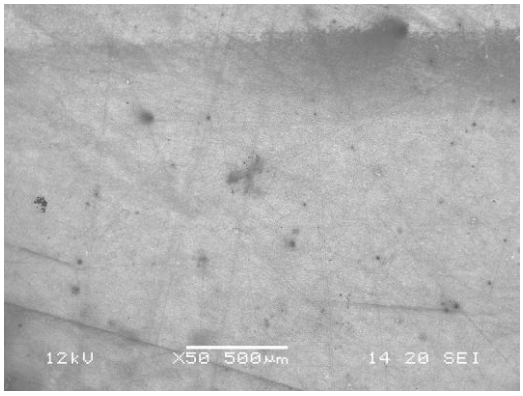

Figure 7.1.18. Al coated surface washed in 0.5M HCl

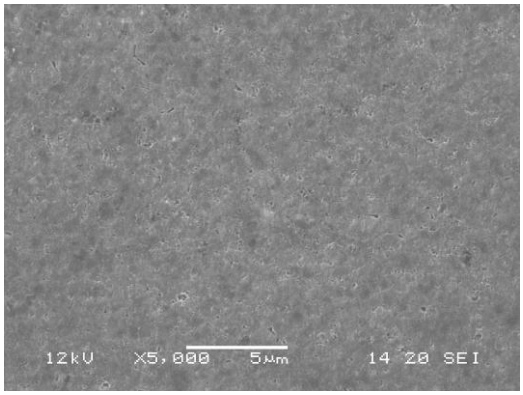

Figure 7.1.19. Al coated surface washed in 1M HCl

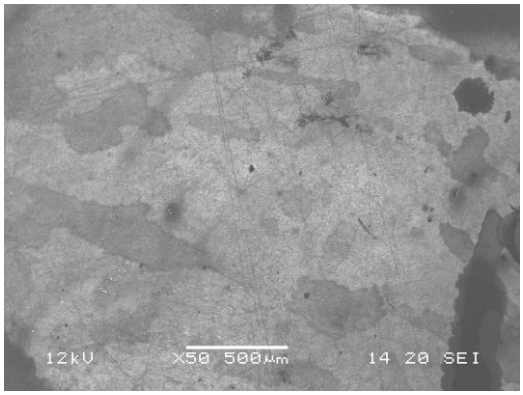

Figure 7.1.20. Al coated surface washed in 1M HCl

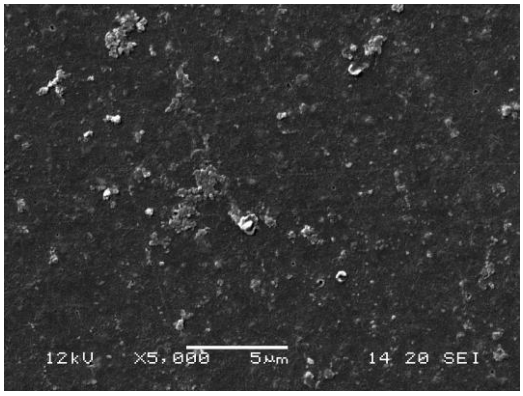

Figure 7.1.21. Unwashed Ni coated surface

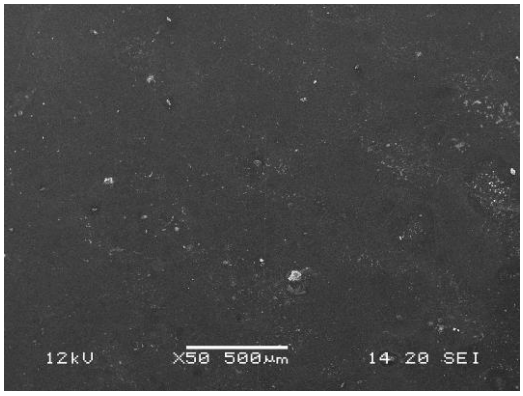

Figure 7.1.22. Unwashed Ni coated surface

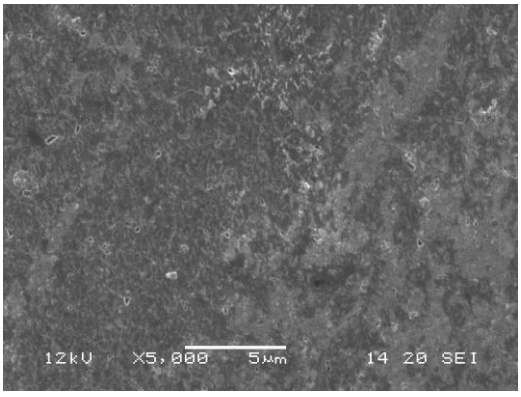

Figure 7.1.23. Ni coated surface washed in 0.25M HCl

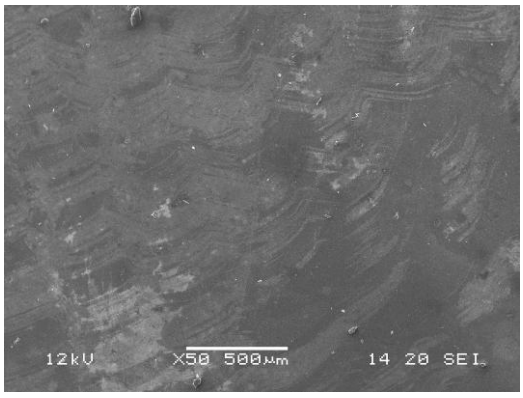

Figure 7.1.24. Ni coated surface washed in 0.25M HCl

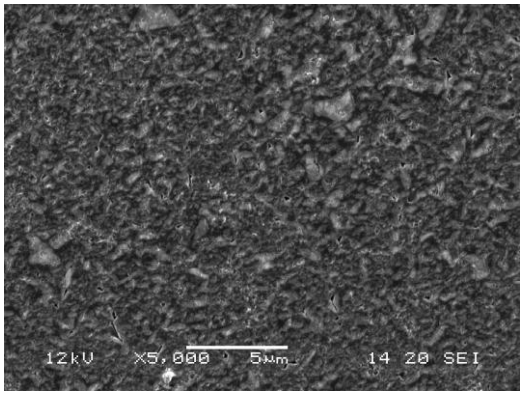

Figure 7.1.25. Ni coated surface washed in 0.5M HCl

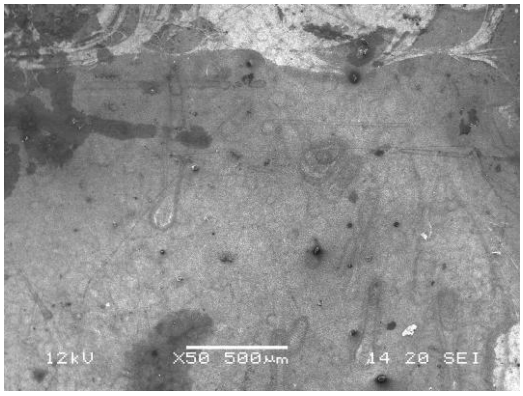

Figure 7.1.26. Ni coated surface washed in 0.5M HCl

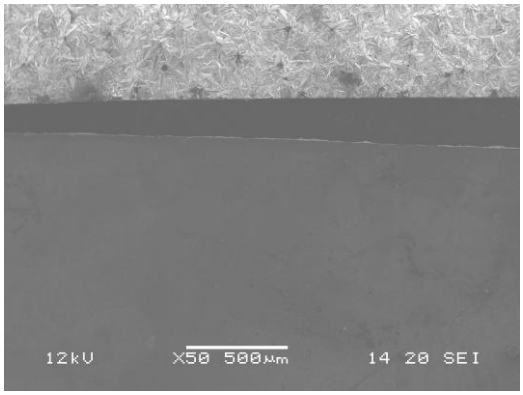

Figure 7.1.27. Mg coated rough surface (top) and Ti coated surface washed in 4M HCl (bottom)

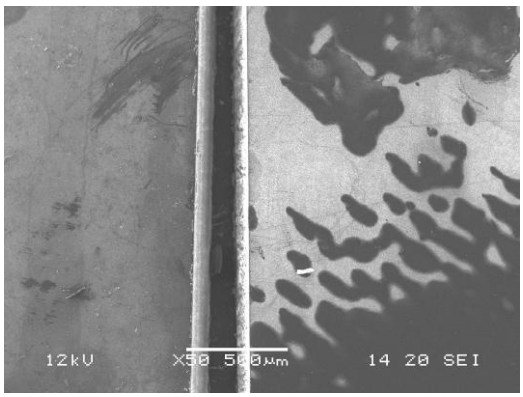

Figure 7.1.28. Ti coated surface washed in 4M HCl (left) and Mg coated smooth surface (right)

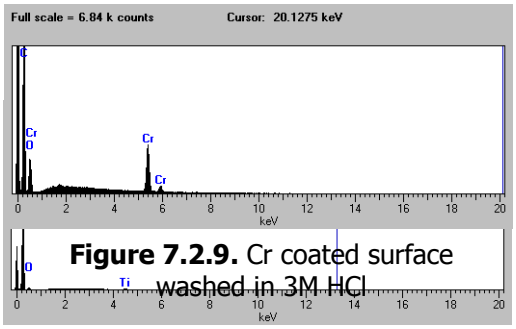

Figure 7.2.9. Cr coated surface washed in 3M HCl

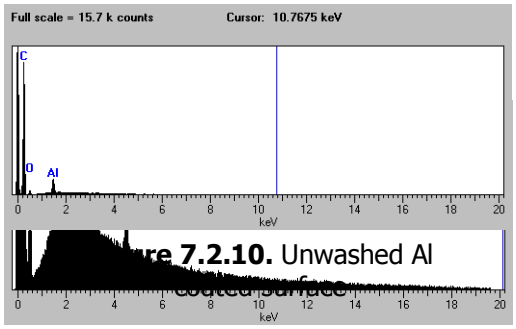

Figure 7.2.10. Unwashed Al coated surface

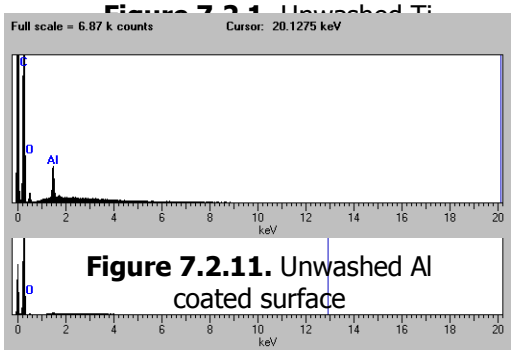

Figure 7.2.11. Unwashed Al coated surface

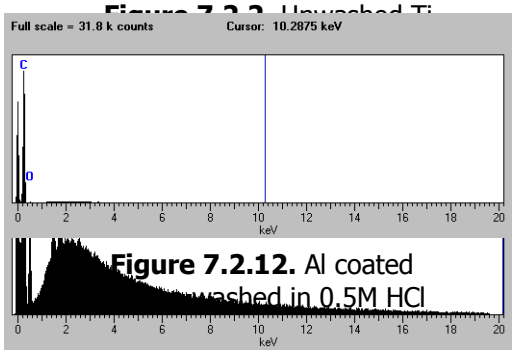

Figure 7.2.12. Al coated washed in 0.5M HCl

Figure 7.2.3. Ti coated surface

Figure 7.2.4. Ti coated surface

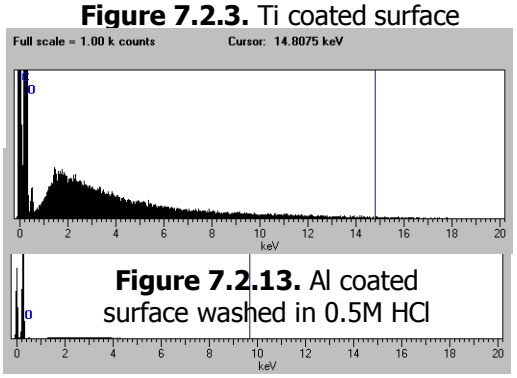

Figure 7.2.13. Al coated surface washed in 0.5M HCl

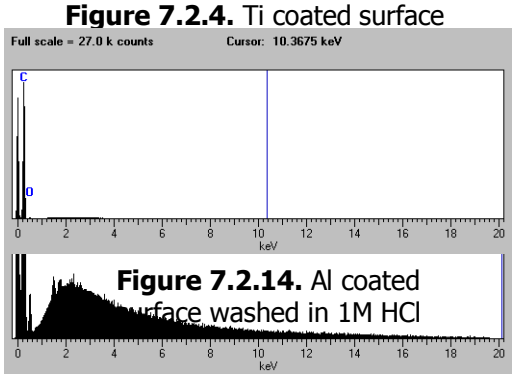

Figure 7.2.14. Al coated surface washed in 1M HCl

Figure 7.2.5. Ti coated surface

Figure 7.2.6. Ti coated surface

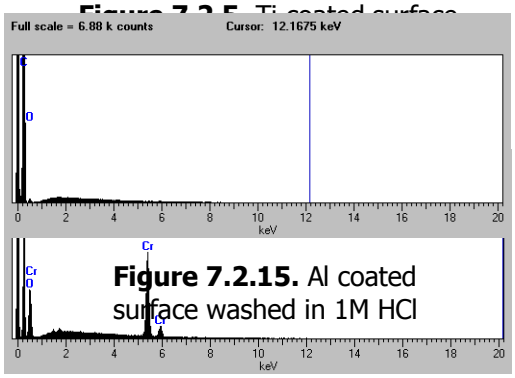

Figure 7.2.15. Al coated surface washed in 1M HCl

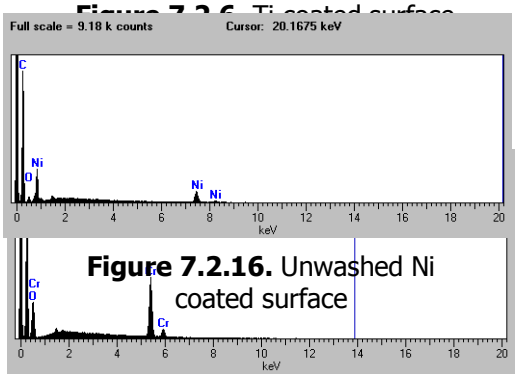

Figure 7.2.16. Unwashed Ni coated surface

Figure 7.2.7. Unwashed Cr coated surface

Figure 7.2.8. Cr coated surface washed in 2M HCl

7.2 – EDX data

7.3 – Raman spectra

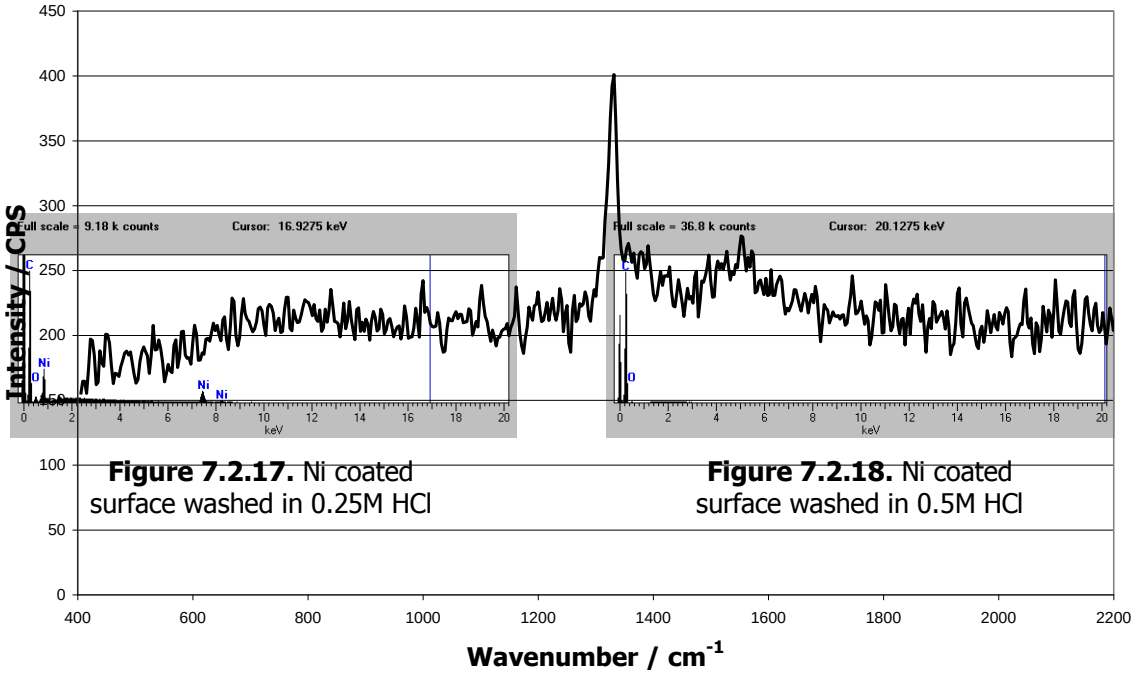

Figure 7.2.17. Ni coated surface washed in 0.25M HCl

Figure 7.2.18. Ni coated surface washed in 0.5M HCl

Figure 7.3.1. Raman spectra of H-terminated diamond sample

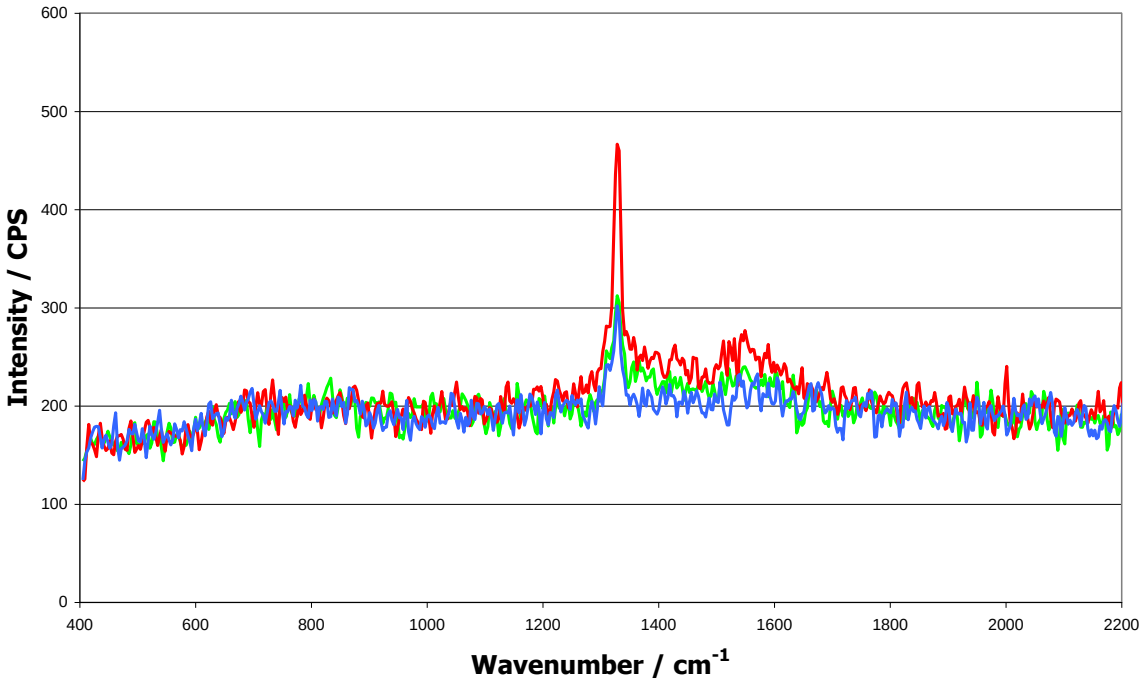

Figure 7.3.2. Raman spectra of Ti coated diamond samples; unwashed in

blue, washed in 4M HCl in red and washed in 2M HCl in green.

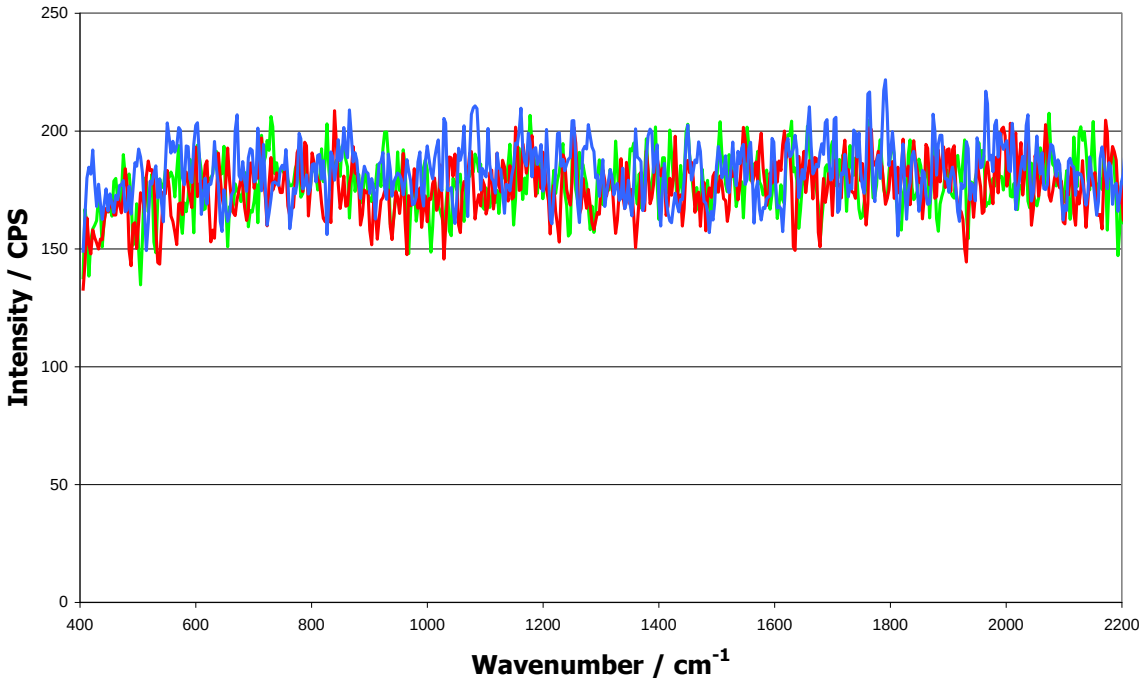

Figure 7.3.3. Raman spectra of Cr coated diamond samples; unwashed in blue, washed in 3M HCl in red and washed in 2M HCl in green.

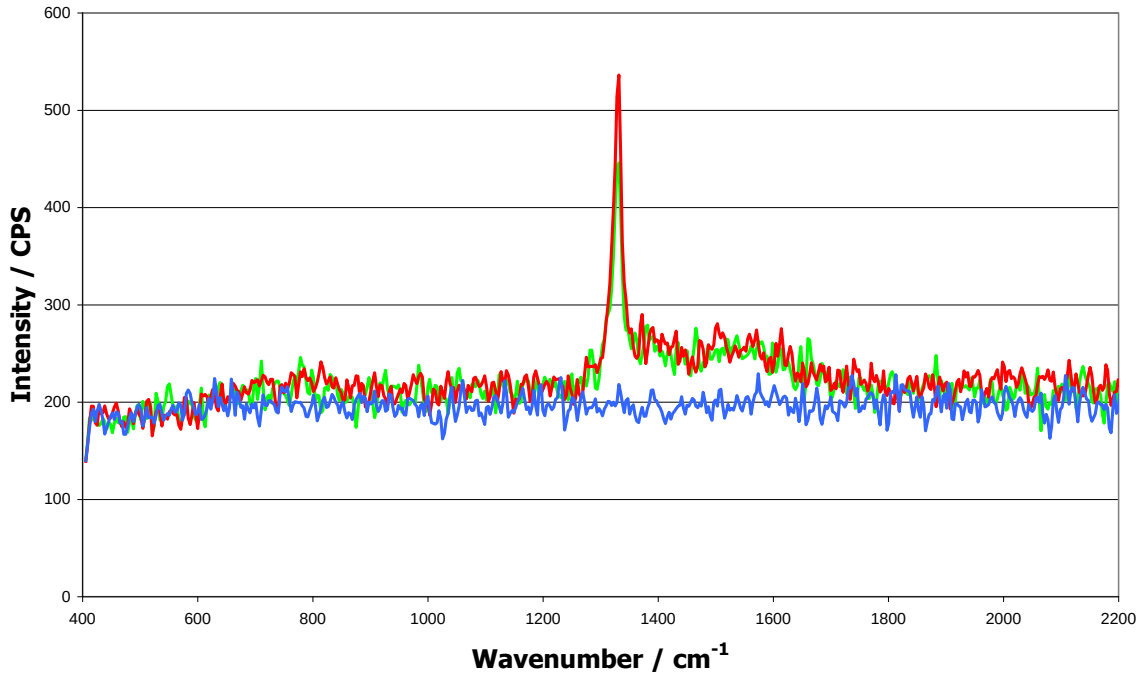

Figure 7.3.4. Raman spectra of Ni coated diamond samples; unwashed in blue, washed in 0.25M HCl in red and washed in 0.5M HCl in green.

7.4 – AFM data

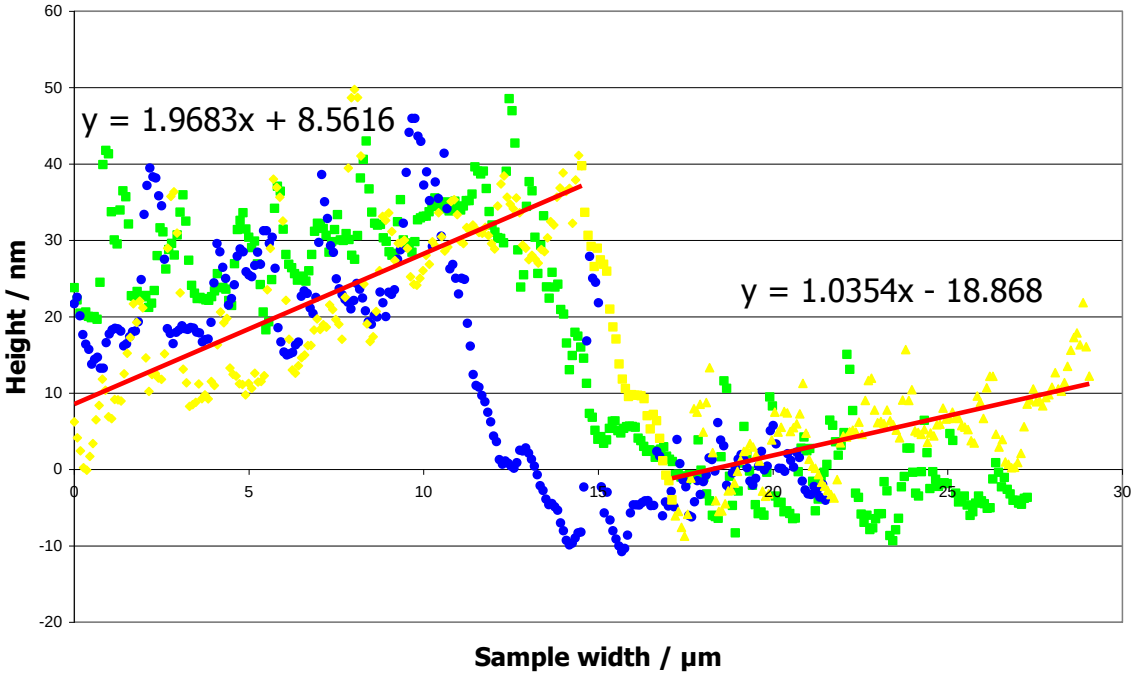

Figure 7.4.1. AFM data for Ti with equations to calculate the step size of metal and hence the thickness of the coating on the diamond samples.

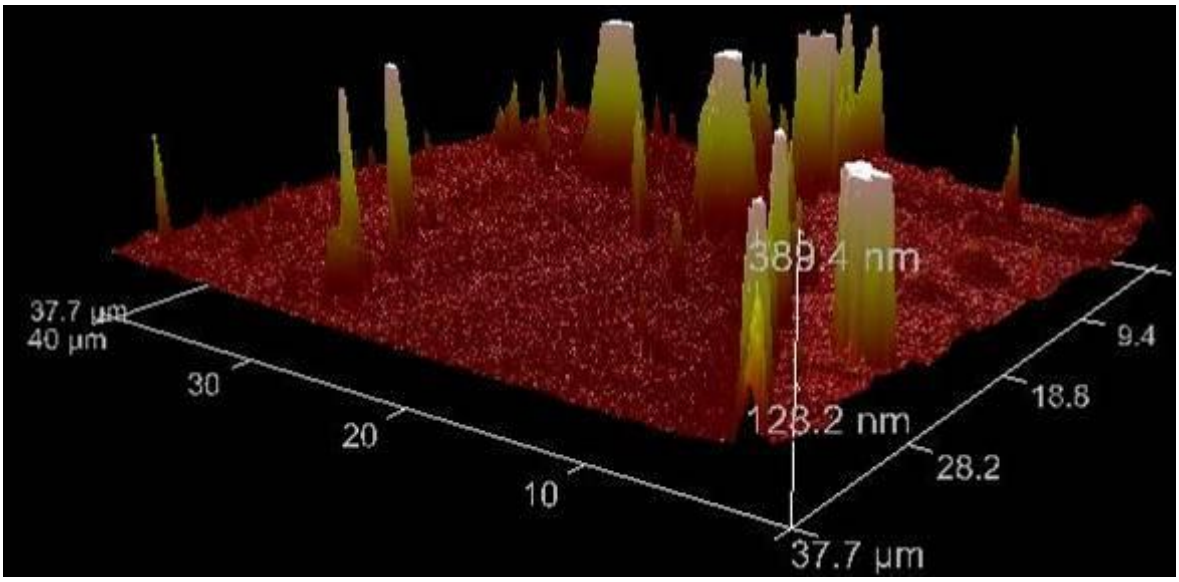

Figure 7.4.2. AFM data for Cr represented in 3D.

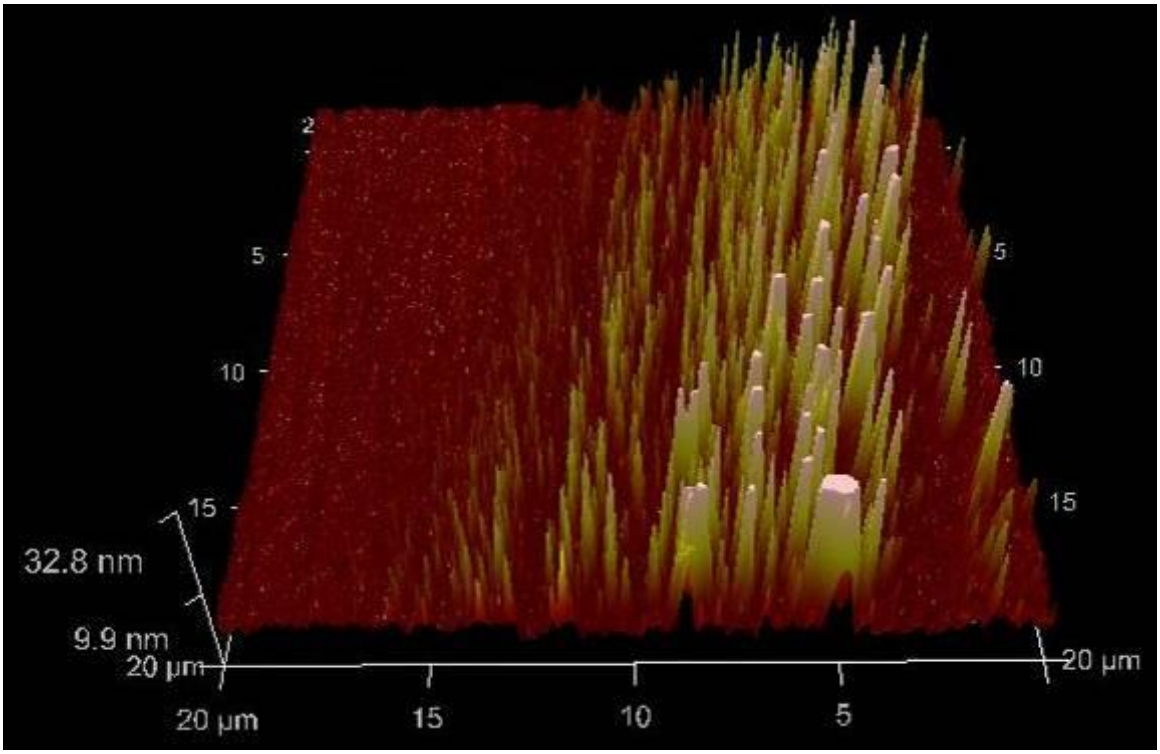
2
5
10
15
32.8 nm
9.9 nm
20 µm
20 µm
15
10
5
5
10
15
20 µm

Figure 7.4.3. AFM data for Ni represented in 3D.

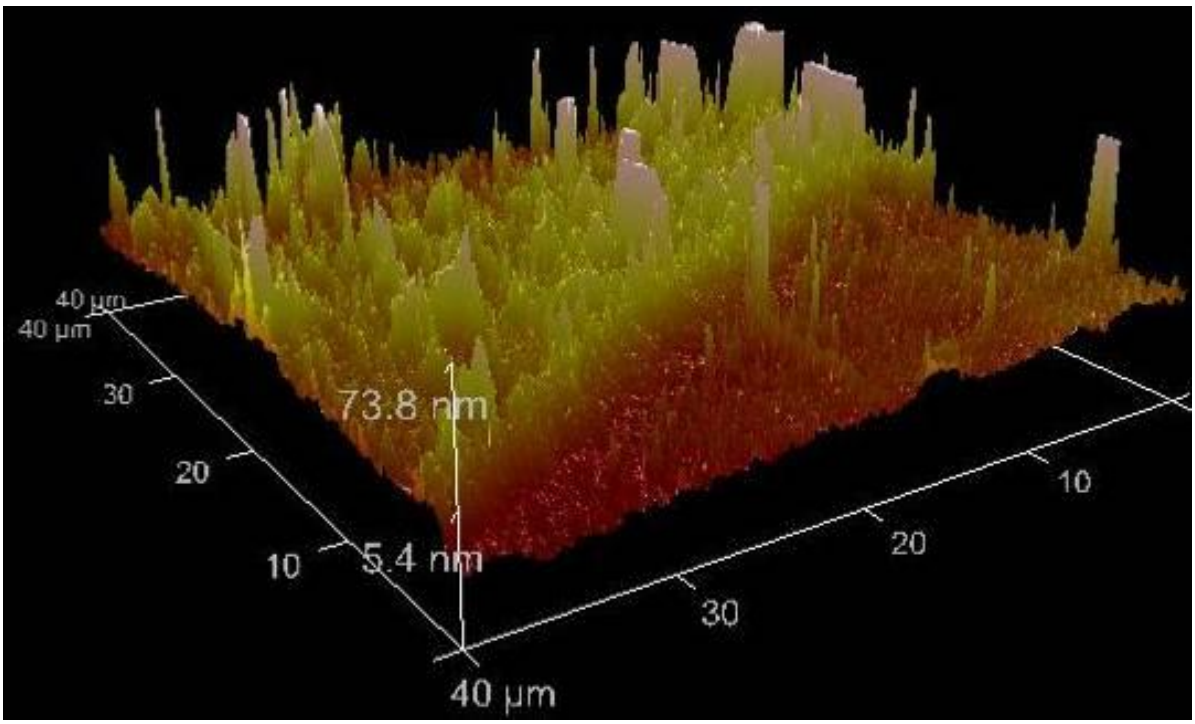

Figure 7.4.4. AFM data for Ti represented in 3D.

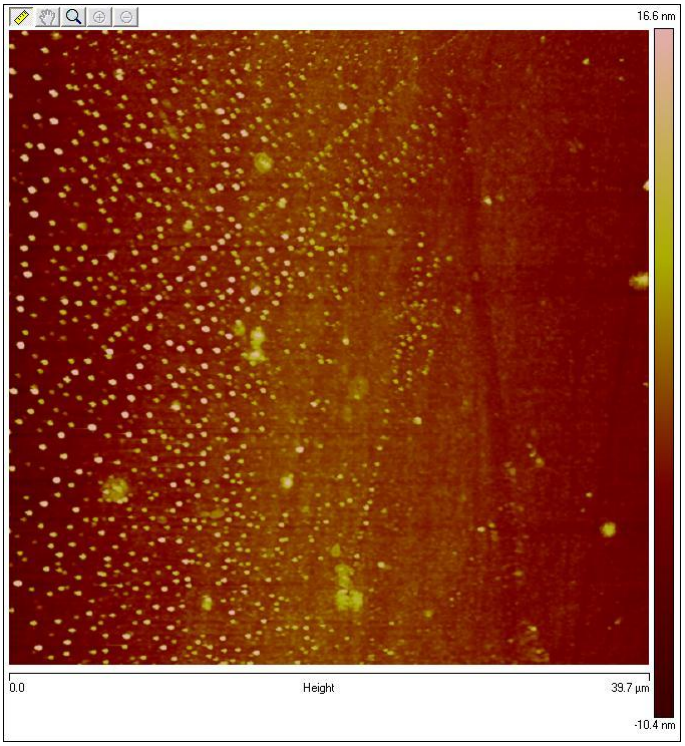

Figure 7.4.5. AFM data for Al represented in 2D.

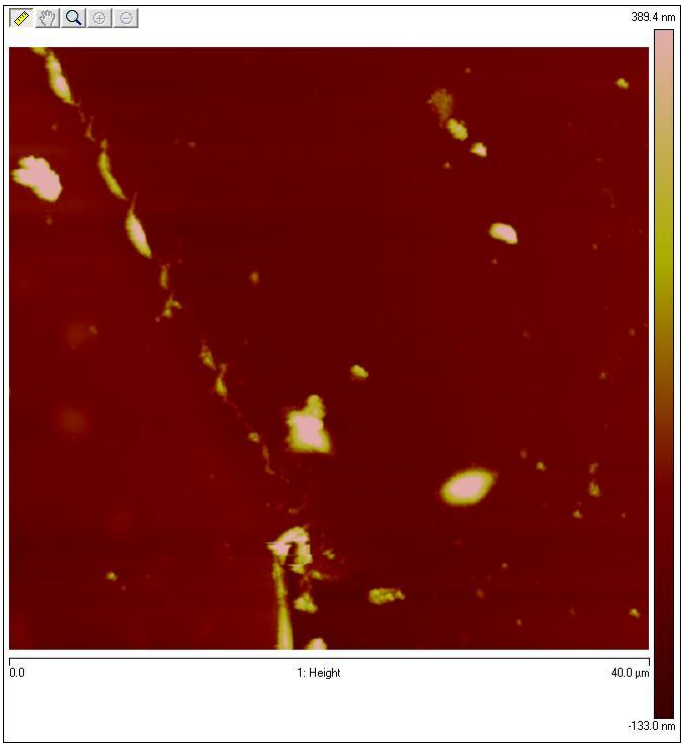

Figure 7.4.6. AFM data for Cr represented in 2D.

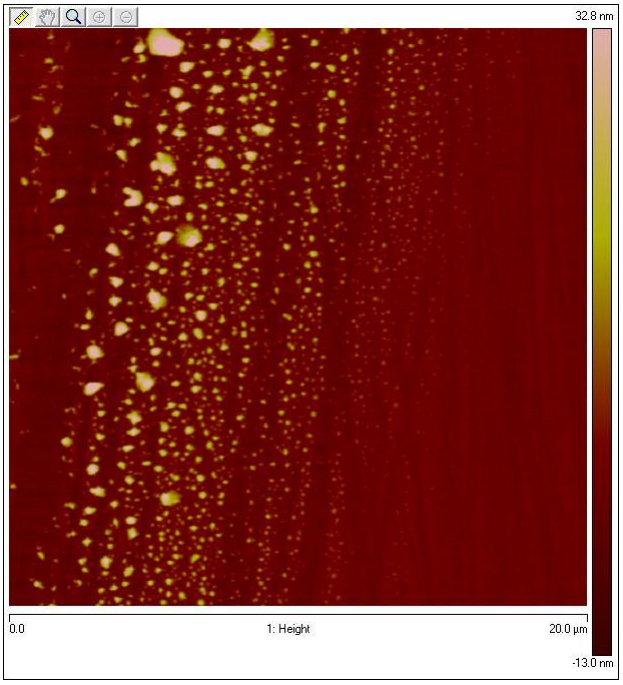

Figure 7.4.7. AFM data for Ni represented in 2D.

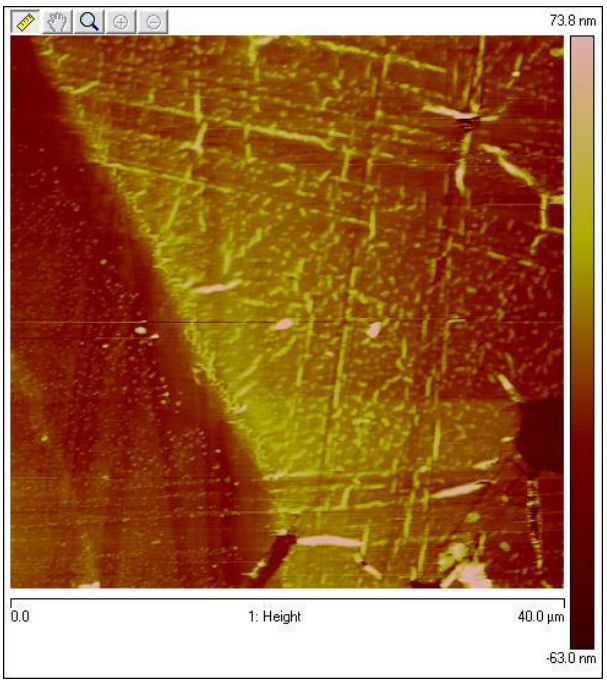

Figure 7.4.8. AFM data for Ti represented in 2D.

8.0 – References

1. R. M. Hazen, *The new alchemists : breaking through the barriers of high pressure*, 1st edn., Times Books, New York, 1993.
2. I. L. Orlov, *The mineralogy of diamond*, Wiley, New York, 1977.
3. R. Berman, *Physical properties of diamond*, Clarendon Press, Oxford, 1965.
4. G. Davies and Institution of Electrical Engineers., *Properties and growth of diamond*, Institution of Electrical Engineers, London, 1994.
5. P. John, N. Polwart, C. E. Troupe and J. I. B. Wilson, *Diamond and Related Materials*, 2002, **11**, 861-866.
6. T. Evans and P. F. James, *Proceedings of the Royal Society of London. Series A. Mathematical and Physical Sciences*, 1964, **277**, 260-269.
7. A. R. Patel and S. Ramanathan, *Philosophical Magazine*, 1962, **7**, 1305-1314.
8. E. Anastassakis, A. Cantarero and M. Cardona, *Physical Review B*, 1990, **41**, 7529-7535.
9. Y. Takano, T. Takenouchi, S. Ishii, S. Ueda, T. Okutsu, I. Sakaguchi, H. Umezawa, H. Kawarada and M. Tachiki, *Diamond and Related Materials*, 2007, **16**, 911-914.
10. S. H. Yang, D. A. Drabold and J. B. Adams, *Physical Review B*, 1993, **48**, 5261-5264.
11. S. P. Mehandru and A. B. Anderson, *Surface Science*, 1991, **248**, 369-381.
12. B. D. Thoms and J. E. Butler, *Surface Science*, 1995, **328**, 291-301.
13. H. Liu and D. S. Dandy, *Diamond chemical vapor deposition : nucleation and early growth stages*, Noyes Publications, Park Ridge, N.J., 1995.
14. M. J. Rutter and J. Robertson, *Physical Review B*, 1998, **57**, 9241-9245.
15. R. U. Martinelli and D. G. Fisher, *Proceedings of the IEEE*, 1974, **62**, 1339-1360.
16. A. Many, Y. Goldstein and N. B. Grover, *Semiconductor surfaces*, North-Holland Pub. Co.; New York, Interscience Publishers, Amsterdam,, 1965.
17. B. F. Williams and J. J. Tietjen, *Proceedings of the IEEE*, 1971, **59**, 1489-1497.
18. R. E. Simons, ed. U. S. A. R. a. D. Labs., Monmouth, N.J., Editon edn., 1963.
19. R. U. Martinelli, *Applied Physics Letters*, 1970, **16**, 261-262.
20. F. J. Himpsel, J. A. Knapp, J. A. VanVechten and D. E. Eastman, *Physical Review B*, 1979, **20**, 624-627.
21. J. van der Weide, Z. Zhang, P. K. Baumann, M. G. Wensell, J. Bernholc and R. J. Nemanich, *Physical Review B*, 1994, **50**, 5803-5806.
22. J. B. Cui, J. Ristein and L. Ley, *Physical Review Letters*, 1998, **81**, 429-432.
23. F. Maier, J. Ristein and L. Ley, *Physical Review B*, 2001, **64**, 165411.
24. D. Takeuchi, C. E. Nebel and S. Yamasaki, *J. Appl. Phys.*, 2006, **99**, 086102.
25. P. K. Baumann and R. J. Nemanich, *Surface Science*, 1998, **409**, 320-335.
26. L. Diederich, O. M. Küttel, P. Aebi and L. Schlapbach, *Surface Science*, 1998, **418**, 219-239.
27. C. Bandis and B. B. Pate, *Surface Science*, 1996, **350**, 315-321.
28. Y. M. Wang, K. W. Wong, S. T. Lee, M. Nishitani-Gamo, I. Sakaguchi, K. P. Loh and T. Ando, *Diamond and Related Materials*, 2000, **9**, 1582-1590.
29. L. Diederich, P. Aebi, O. M. Küttel and L. Schlapbach, *Surface Science*, 1999, **424**, L314-L320.
30. W. E. Pickett, *Physical Review Letters*, 1994, **73**, 1664-1667.
31. M. W. Geis, J. A. Gregory and B. B. Pate, *Electron Devices, IEEE Transactions on*, 1991, **38**, 619-626.
32. C. Bandis and B. B. Pate, *Physical Review B*, 1995, **52**, 12056-12071.
33. K. G. Hernqvist, M. Kaneisky and F. H. Norman, *RCA Review*, 1958, 224.
34. G. M. Gryaznov, E. E. Zhabotinskii, A. V. Zrodnikov, Y. V. Nikolaev, N. N. Ponomarev-Stepnoi, V. Y. Pupko, V. I. Serbin and V. A. Usov, *Atomic Energy*, 1989, **66**, 414-418.
35. K. P. Loh, J. S. Foord, R. G. Egdell and R. B. Jackman, *Diamond and Related Materials*, 1997, **6**, 874-878.
36. M. W. Geis, J. C. Twichell, J. Macaulay and K. Okano, *Applied Physics Letters*, 1995, **67**, 1328-1330.
37. M. Suzuki, T. Ono, N. Sakuma and T. Sakai, *Diamond and Related Materials*, 2009, **18**, 1274-1277.

38. M. Kataoka, C. Zhu, F. A. M. Koeck and R. J. Nemanich, *Diamond and Related Materials*, 2009, **19**, 110-113.
39. K. M. O'Donnell, T. L. Martin, N. A. Fox and D. Cherns, *Physical Review B*, 2010, **82**, 115303.
40. W. Shockley and H. J. Queisser, *Journal of Applied Physics*, 1961, **32**, 510-519.
41. M. W. Geis, J. C. Twichell and T. M. Lyszczarz, *Journal of Vacuum Science & Technology B*, 1996, **14**, 2060-2067.
42. T. Sakai, T. Ono, N. Sakuma, M. Suzuki and H. Yoshida, *New Diamond and Frontier Carbon Technology*, 2007, **17**, 189.
43. G. T. Mearini, I. L. Krainsky, J. J. A. Dayton, Y. Wang, C. A. Zorman, J. C. Angus, R. W. Hoffman and D. F. Anderson, *Applied Physics Letters*, 1995, **66**, 242-244.
44. R. S. Sussmann, *CVD diamond for electronic devices and sensors*, Wiley, Chichester, 2009.
45. P. May, *Surfaces and their Characterisation*, http://www.chm.bris.ac.uk/~paulmay/misc/molesurf/section2.htm.
46. A. M. Zaitsev, *Optical properties of diamond : a data handbook*, Springer, Berlin ; New York, 2001.